Schweizerische Eidgenossenschaft
Confédération suisse
Confederazione Svizzera
Confederaziun svizra

Federal Department of the Environment, Transport, Energy and Communications DETEC

Swiss Federal Office of Energy SFOE
Energy Research and Cleantech Division

Final report dated 04.09.2023

Improving the energy efficiency of grinding processes with fast and efficient simulation tool --- using rail grinding as a case study

Source: EtiAmmos/shutterstock.com

Date: 04.09.2023

Location: Bern

Publisher:
Swiss Federal Office of Energy SFOE
Energy Research and Cleantech
CH-3003 Bern
www.bfe.admin.ch

Subsidy recipients:
inspire AG
Technoparkstrasse 1, 8005 Zürich
https://www.inspire.ethz.ch/

Authors:
Michal Kuffa, Michal.kuffa@inspire.ch

SFOE project coordinators:
Carina Alles, Carina.Alles@bfe.admin.ch
Simone Marchesi

SFOE contract number: SI/502466-01

Zusammenfassung

Schleifen ist ein energieintensiver Prozess. Als weltweit führender Exporteur von Schleifmaschinen ist es für die Schweiz wichtig, einen energieeffizienten Schleifprozess zu haben. Das Projekt RESI konzentriert sich auf die Verbesserung der Energieeffizienz im Schienenschleifprozess unter Verwendung der von inspire AG und IWF, ETH Zürich, gemeinsam entwickelten Simulationssoftware iBRUS. Dies soll durch die Auswahl der optimalen Prozessparameter erreicht werden. Das Gesamtprojekt ist in 6 Arbeitspakete unterteilt. Der vorliegende Bericht fasst die Arbeiten der Arbeitspakete 1-4 zusammen.

Die Entwicklung eines kinematisch-geometrischen Simulationswerkzeuges ermöglicht die präzise Abschätzung des Materialabtrags von Einzelkornkratzern mit einer Fehlermarge von nur 6%. Diese Simulationsechnik erlaubt die Anpassung der Schleifkräfte an das Kienzle-Kraftmodell und eröffnet die Simulation von Materialabtrag und Kraftprofilen unter Verwendung von Schleifscheiben mit mehreren Körnern.

Das Ergebnis der Arbeit zeigt die Robustheit des Materialabtrags bezüglich Zeitschrittgröße und der Werkstückauflösung. Darüber hinaus kann festgestellt werden, dass der spezifische Energieverbrauchs mit Hilfe von iBRUS im voraus geschätzt werden kann. Diese Abschätzung wird jedoch nie exakt sein, da es zu viele Unsicherheiten in den Experimenten für die Modellkalibierung gibt, die wiederum zu Abweichungen der Ergebnisse in den Simulationen führen.

Durch Anpassungen der Prozessparameter – Schnittgeschwindigkeit und Vorschub konnte eine Einsparung des Energieverbrauchs von bis zu 12%. erreicht werden. Diese Einsparung ist jedoch abhängig von einem Modell für die Schnitttiefe und gilt nur für einen bestimmten Bereich. Da der Prozess des Schienenschleifens viele technische Eigenheiten aufweist, die in einer Simulation nur schwer zu beschreiben sind, gelten die Ergebnisse auch nur für die quasi-stationäre Phase des Prozesses. Nicht untersucht wurde ob die zur Minimierung des Energieverbrauchs gefundenen Parameter zu Schleifbrand führen können.

Eine generelle Schlussfolgerung ist dass höhere Spindeldrehzahlen den Energieverbrauch senken, während höhere Vorschubgeschwindigkeiten den Energieverbrauch erhöhen. Die Grenze für höhere Spindeldrehzahlen wird durch die Schleifscheibe gesetzt, die bei zu hohen Drehzahlen versagen kann.

Abschliessend lässt sich sagen, dass die Simulationen aus diesem Projekt erhebliche Fortschritte bei der Verbesserung der Energieeffizienz des Schienenschleifprozesses aufzeigen. Allerdings bleiben zu mehreren wichtige Aspekten - darunter die konstante Normalkraft, Nichtlinearitäten im Schnitttiefenmodell und das Potenzial für Schleifbrand - offene Fragen, die eine weitere experimentelle Validierung und eventuell die Neukonstruktion der Schleifwerkzeuge erfordern bevor die erwarteten Energieeinsparungen voll ausgeschöpft werden können. Aufgrund begrenzter Zeit und Ressourcen wurde der Schwerpunkt dieses Projektes darauf gelegt, die optimalen Prozessparameter für das in der Praxis am häufigsten verwendete Werkzeug zu finden. Damit wird eine bessere Ausganslage für weitere Schritte wie die Entwicklung neuer Schleifscheiben und deren Einsatz in Feldversuchen geschaffen.

Résumé

Le meulage est un processus énergivore. En tant que principal exportateur mondial de machines à rectifier, il est important pour la Suisse d'avoir un processus de meulage écoénergétique. Le projet RESI se concentre sur l'amélioration de l'efficacité énergétique dans le processus de meulage des rails en utilisant le logiciel de simulation iBRUS développé en collaboration par inspire AG et IWF de l'ETH de Zurich. Cela sera accompli en choisissant les paramètres de processus optimaux. Le projet global est divisé en 6 packages de travail. Le présent rapport résume les travaux des packages de travail 1 à 4.

Le développement d'un outil de simulation géométrique cinématique permet une estimation précise de l'enlèvement de matière des rayures à grain unique avec une marge d'erreur de seulement 6%. Cette technique de simulation permet d'ajuster les forces de meulage au modèle de force de Kienzle et ouvre la voie à la simulation de l'enlèvement de matière et des profils de force en utilisant des meules composées de plusieurs grains.

Les résultats du travail montrent la robustesse de l'enlèvement de matière par rapport à la taille des pas de temps et à la résolution de la pièce. De plus, il est possible d'estimer à l'avance la consommation d'énergie spécifique à l'aide d'iBRUS. Cependant, cette estimation ne sera jamais exacte car il existe trop d'incertitudes dans les expériences pour l'étalonnage du modèle, ce qui conduit à des écarts entre les résultats des simulations.

En ajustant les paramètres du processus - vitesse de coupe et avance -, une économie de consommation d'énergie pouvant atteindre 12% a été obtenue. Cependant, cette économie dépend d'un modèle de profondeur de coupe et ne s'applique qu'à une plage spécifique. Étant donné que le processus de meulage des rails présente de nombreuses caractéristiques techniques difficiles à décrire dans une simulation, les résultats ne s'appliquent également qu'à la phase quasi stationnaire du processus. Il n'a pas été étudié si les paramètres trouvés pour minimiser la consommation d'énergie peuvent entraîner un emballement de meulage.

Une conclusion générale est que des vitesses de broche plus élevées réduisent la consommation d'énergie, tandis que des avances plus élevées augmentent la consommation d'énergie. La limite de vitesses de broche plus élevées est déterminée par la meule, qui peut échouer à des vitesses trop élevées.

En conclusion, les simulations de ce projet montrent des progrès significatifs dans l'amélioration de l'efficacité énergétique du processus de meulage des rails. Cependant, plusieurs aspects importants - notamment la force normale constante, les non-linéarités dans le modèle de profondeur de coupe et le potentiel d'emballement de meulage - restent des questions ouvertes qui nécessitent une validation expérimentale supplémentaire et éventuellement une nouvelle conception des outils de meulage avant que les économies d'énergie attendues puissent être pleinement exploitées. En raison de contraintes de temps et de ressources, l'accent de ce projet a été mis sur la recherche des paramètres de processus optimaux pour l'outil le plus couramment utilisé en pratique. Cela crée une base solide pour les étapes ultérieures, telles que le développement de nouvelles meules et leur utilisation dans des essais sur le terrain.

.

Summary

Grinding is an energy-intensive process. As the world's leading exporter of grinding machines, it is important for Switzerland to have an energy-efficient grinding process. The RESI project focuses on improving energy efficiency in the rail grinding process using the iBRUS simulation software developed in collaboration by inspire AG and IWF at ETH Zurich. This will be achieved by selecting optimal process parameters. The overall project is divided into 6 work packages. This report summarizes the work of work packages 1 to 4.

The development of a kinematic-geometric simulation tool enables precise estimation of material removal from single-grain scratches with a margin of error of only 6%. This simulation technique allows adjustment of grinding forces to the Kienzle force model and opens the way for simulation of material removal and force profiles using grinding wheels with multiple grains.

The results of the work show the robustness of material removal with respect to time step size and workpiece resolution. Furthermore, it can be noted that the specific energy consumption can be

estimated in advance using iBRUS. However, this estimate will never be exact as there are too many uncertainties in the experiments for model calibration, leading to deviations in simulation results.

By adjusting process parameters - cutting speed and feed rate - an energy consumption saving of up to 12% was achieved. However, this saving depends on a depth of cut model and only applies to a specific range. Given that the rail grinding process has many technical peculiarities that are difficult to describe in a simulation, the results also apply only to the quasi-stationary phase of the process. It was not investigated whether the parameters found to minimize energy consumption can lead to grinding burn.

A general conclusion is that higher spindle speeds reduce energy consumption, while higher feed rates increase energy consumption. The limit for higher spindle speeds is determined by the grinding wheel, which can fail at too high speeds.

In conclusion, the simulations from this project show significant progress in improving the energy efficiency of the rail grinding process. However, several important aspects - including constant normal force, nonlinearities in the depth of cut model, and the potential for grinding burn - remain open questions that require further experimental validation and possibly the redesign of grinding tools before the expected energy savings can be fully realized. Due to limited time and resources, the focus of this project was on finding the optimal process parameters for the most commonly used tool in practice. This creates a solid foundation for further steps, such as the development of new grinding wheels and their use in field trials.

Main Findings

- Kinematic geometric simulation tools were developed to estimate material removal of single-grain scratches within a limited error range of 6%. Ggrinding forces were found to closely align with the Kienzle force model. Such modeling techniques will enable simulation of material removal and force profiles with grinding wheels consisting of multiple grains.
- Estimating grinding temperature is not straightforward using the discussed Takazawa model, which predicts the maximum flash temperature of a single grain. The validation of these results against experimental data remains uncertain.
- Energy results are significantly reliant on process parameters, emphasizing the critical need for proper parameter selection to optimize energy efficiency.
- Investigating grinding outcomes across various feed rates, depths of cut, and spindle speeds confirms an indirect linear relationship between depth of cut and feed rate, as well as a direct linear relationship between depth of cut and spindle speed.
- By adjusting the feed rate and cutting speed, the study successfully achieved a notable nearly 12% reduction in spindle power consumption.
- Extension of the scope of this project from process parameter optimization to tool parameter optimization opens more room for further estimation of energy savings for a defined grinding job.

Contents

Abbreviations

List of Abbreviations

Olga	The rail grinding experimental setup in Technopark
MRM	Material removal model in iBRUS simulation

List of Symbols

Symbol	Measuring unit	Description
a_p	mm	Depth of cut
k_c	N/mm²	Specific cutting force or specific energy
F_c	N	Tool cutting force
$A_{cut,i,j}$	mm	Cutting area for grain i at simulation step j
P_{cut}	Watt	Cutting power
ω	radiant/s	Spindle rotational speed, rotational speed of grinding wheel
ω_w	radiant/s	Rotational speed of workpiece ring on Olga test bench
R	mm	Average grinding wheel radius
U	Volt	Voltage needed for grinding process
I	Ampere	Electrical current
P_E	Watt	Electrical power
P_{ml}	Watt	Total mechanical power loss
P_{el}	Watt	Total electrical power loss
M	Nm	Grinding wheel torque
N	-	Number of grains in grinding wheel
T	-	Number of simulation steps in one iBRUS simulation
W_W	mm	Width of workpiece
L	mm	Grinded length of workpiece
r_i	mm	Inner radius of grinding wheel
r_a	mm	Outer radius of grinding wheel
E_{sim}	Joule	Energy consumption calculated in simulation
E_{exp}	Joule	Energy consumption calculated based on experimental data
V_{sim}	mm³	Removed material volume in simulation
V_{exp}	mm³	Removed material volume in experiment
v_f	m/s	Feed speed of workpiece
v_c	m/s	Tool cutting speed of grinding wheel
F_{c_sim}	N	Tool cutting force simulated in simulation
F_{c_exp}	N	Tool cutting force measured in experiment
F_{N_exp}	N	Tool cutting force set in experiment
F_{N_sim}	N	Tool normal force simulated in simulation

1 Introduction

1.1 Background information and current technology status

1. The grinding process is particularly energy-intensive among abrasive processes.

According to Rowe, W. B [1], the energy required in grinding is more than 10 times higher than the shear flow stress in the material. Compared to the other metal-cutting operations, the specific energies for grinding were stated in Malkin, & Guo, C. [2] to be much higher and getting even larger in fine grinding.

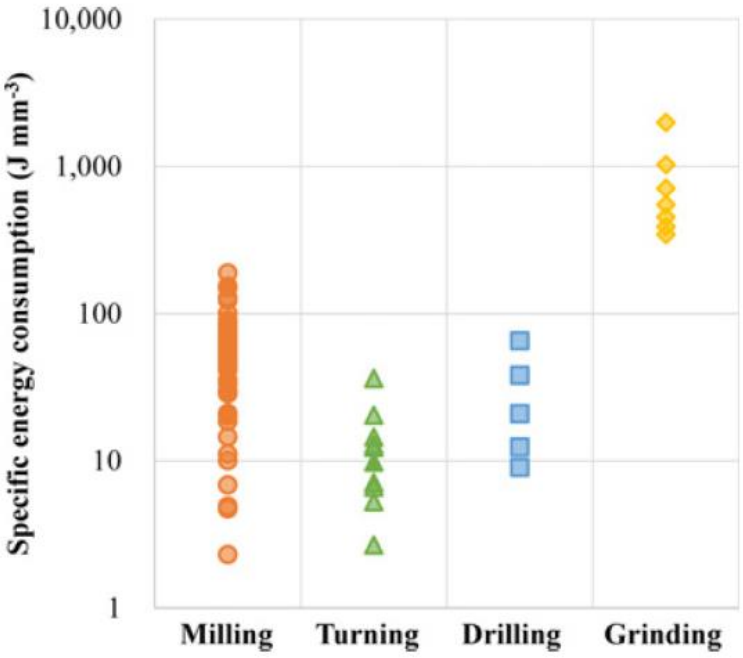

Figure 1 Energy consumption comparison between different abrasive processes [3]

The energy consumption in grinding is also influenced by the material removal rate, which is lower for grinding than other processes like milling or turning. This makes specific energy requirements of grinding ranging around 300 to 12000 J/mm^3, while according to Yoon et al. [3] for turning or milling the order of magnitude is around 1 to 100 J/mm^3. Another result from the study of Hacksteiner et al. [4] shows that with increasing cutting speed the required spindle speed, thus drive power consumption, increases.

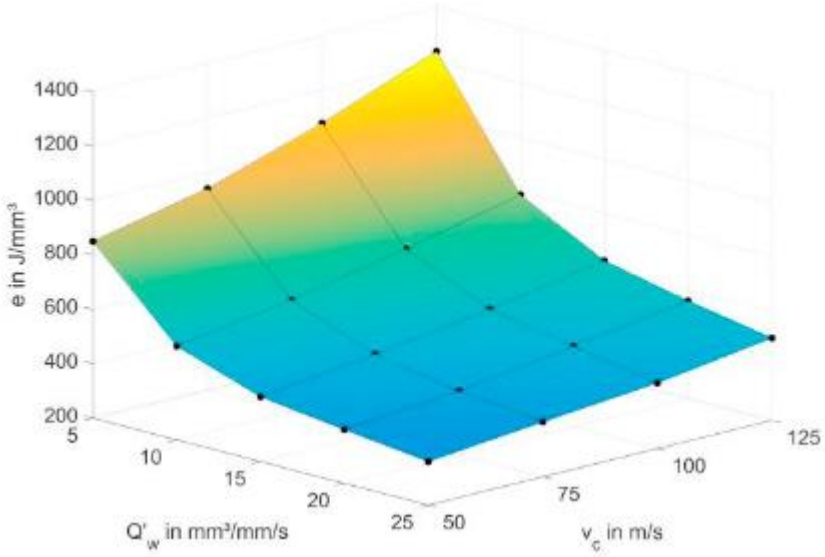

Figure 2 : Dependence of specific energy consumption e on cutting speed v_c and specific material removal rate Q'_w for creep feed grinding [4]

For the wet grinding processes, the energy required for the utilization of the cutting fluid is even higher than the spindle power delivered, as shown in Figure 3.

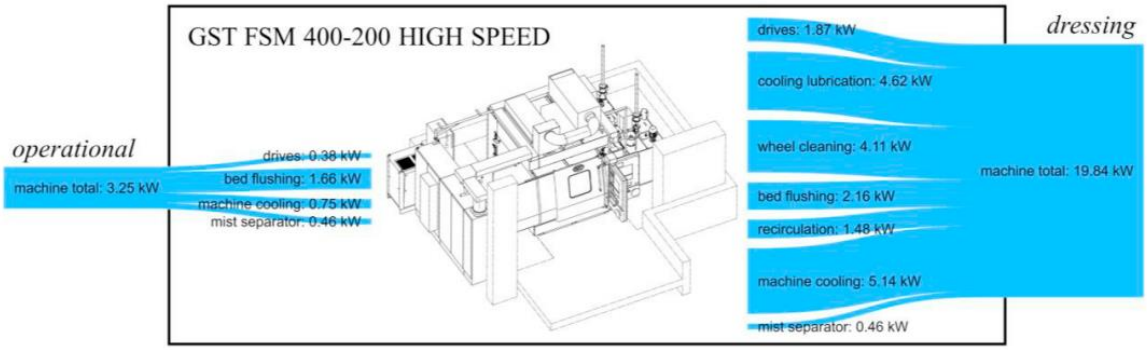

Figure 3 : Electrical power consumption of the grinding machine in 'operational' condition (left) and during dressing (right) [4]

As it is shown, the energy consumption of grinding is considerably high among all machining processes and it depends on many factors, the optimization of these processes carries significant potential for reduction of energy consumption.

On the other hand, it must be noted that the results from above literature research might not necessarily apply to this project, since most of the grinding process presented above are path controlled, while rail grinding is a force controlled process.

In this project, the optimization of energy efficiency is only focused on dry grinding processes. Thus, the energy consumption of cooling from Fig 4 is not within consideration, such as cooling lubrication, machine cooling, etc. The main component to optimize in energy consumption will be the spindle power, where the aim is to reduce this component by optimizing process parameters, such as cutting speed, feed speed and normal force.

2. Grinding processes play an important role in Swiss economy and have environmental impacts in various categories.

According to OEC [5], as of 2019, Switzerland is the 2nd largest exporter of the gear cutting, grinding and finishing machines in the world. Thus, as highlighted in the 2050 Energy Strategy of Switzerland [6], a widely used high-energy process like grinding is naturally a target for achieving the goal of higher energy efficiency. In addition, grinding processes contributes to various categories of environmental impacts. The sustainability improvement potential can be addressed in different categories in the life cycle of grinding processes. As for the tool users, Linke et al. [7] state that the main point of interest is improving the energy use and performance of ground parts, which will be the focus of this project proposal.

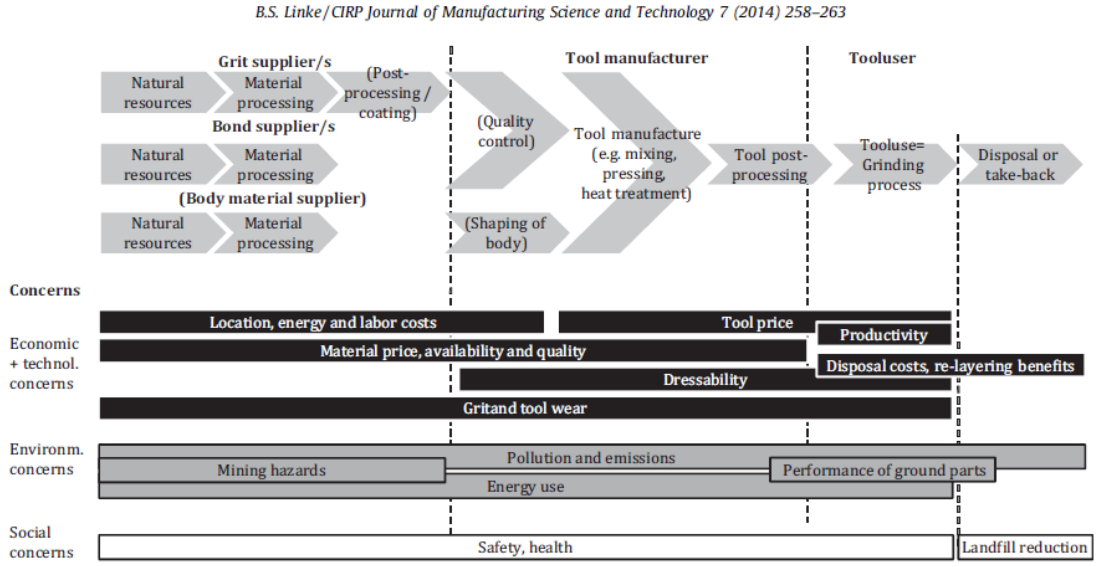

Figure 4 : Environmental impact of grinding processes [7]

3. There is significant potential for improving energy efficiency in machining industry in Switzerland

According to the Swiss Machine, Electrical and Metal industry association Swissmem [8], the total energy consumption of the MEM industry in 2019 was around 17000 TJ, or 4720 GWh. Moreover, according to the survey done in EEM4T project [9], there are currently more than 110'000 machine tools installed in Switzerland, and an average of 23% energy savings for these machines were found possible. The grinding processes are among these machining processes and contribute to the high energy consumption of the industry. However, the exact energy-saving potential for a grinding process is unknown.

1.2 Purpose of the project

An improvement of the energy performance of grinding processes can be achieved by optimizing the process parameters. However, it is a costly process as the knowledge base on grinding in the industry is limited and the manufacturers need to run a large number of experiments to find optimal processes. These practical constraints and time costs prevent industry practitioners to find optimal process parameters efficiently.

Here, a simulation tool for grinding processes is a great replacement for the experiments to optimize grinding processes. A simulation is much less costly than an experiment and gives the manufacturers more flexibility to test and find optimal parameters. At IWF ETH Zürich and inspire AG, numerous research has been done on grinding processes and a great amount of experience has been accumulated. These experiences and knowledge from research activities are channelled to build an in-house simulation tool for grinding processes. This simulation tool enables users to simulate grinding processes in a fast and robust manner compared to conventional simulation techniques such as FEM. It's a versatile tool that provides the possibility for users to build various models on top of the micro-scale geometric model.

The simulation is capable of calculating many process results such as forces, wear, temperature, etc. This, combined with the possibility of expanding the simulation easily, thanks to its versatile structure, gives the possibility to build an energy consumption model for process energy estimation. This research project is proposed to build such a model and use the tool to find the optimal parameter sets which yield the optimum finishing surface quality with the most efficient energy consumption possible.

The parameters for the optimization are selected from the process parameters, such as cutting speed, feed speed, and normal force, in line with the original scope, WP1-4 is devoted to the build-up and enhancement of the energy model in the simulation tool, optimizing for the energy consumption under various feed and spindle speeds and normal forces followed by the validation of such results in lab experiments in WP4.

Based on the interest of the industry partner the scope of the project could be extended in the future to accommodate for tool parameter optimization. This implies the re-application of WP1-3 within a larger scope. Finally, W5-6 should be applied to cross-validate findings from rail grinding at the field (WP5) as well as to quantify the overall energy savings for Switzerland with the enlarged scope of parameter optimization.

Concerning the tool parameter optimization, variation of tool parameters such as grain size, grain shape, grain distributions and tool dimensions are intended.. Tool optimization may lead to further complications since not all the grinding wheels designs suggested by the simulation will be available for testing. This implies that the extension of the project's scope to include tool parameter optimization may lead more into speculation. Yet, it will be interesting to analyze what-if scenarios for various envisioned grinding wheels with different geometrical characteristics.

Due to limitations in time and resources, the focus of this project was shifted towards WP1-4, i.e. identifying the best-suited process parameters for the frequently employed grinding tool, rather than pursuing field tests (WP5) that would be too risky at the current level if insights, or the creation of novel grinding wheels. Work Packages 5 and 6 were eliminated due to the impractical manufacturability of the resin-bonded corundum grinding wheel capable of achieving the required cutting speed of 80 m/s within a realistic timeframe. This would necessitate an entirely new development in collaboration with a grinding wheel manufacturer, a process estimated to take 1-2 years.

Last but not least, once the knowledge base is more robust, the potential of this simulation tool to improve the energy efficiency in rail grinding should be assessed as originally planned in WP6..

1.3 Objectives

The following research questions were listed in the research proposal and serve as a base for the objectives:

Research questions:

1. How can the energy consumption of a grinding process be estimated in a kinematic-geometrical model? (WP1)
2. How much energy can be saved by reducing the spindle power consumption found by the simulation tool in a reference rail grinding setup? (WP3)
3. How accurate is the prediction of energy consumption from the simulation tool compared to the lab experiment? What are the differences between them? (WP2, WP4)
4. Based on the optimized rail grinding process performance, how does the energy-saving measures scale up to rail grinding process and potentially other dry grinding process for Switzerland? (WP6)

Objectives of the entire project as initially planned are listed below in the form of deliverables:

1. Deliverable 1: Enhancement of the simulation tool
    A. Implement single scratch simulation of rail grinding. When varying simulation parameters such as simulation step size and the number of simulation steps, the removed volume variation should be within 20%.
    B. Two models in the iBRUS software: temperature model and energy estimation model

    Challenges:

    A. Direct temperature measurement at the rail grinding face is not possible in the process. The prediction of temperature needs to take an indirect approach, which might affect the accuracy.
    B. Because of the uncertainty brought by the temperature model, the estimate of energy consumption could also be uncertain.
2. Deliverable 2: Simulation of the rail grinding process in the iBRUS software, where
    A. Simulation with 20,000 grains wheel representing 0.1s of rail grinding in real time is completed in 1 hour.
    B. Grinding wheel topology is accurately represented in the software, where the deviation of the Abbott-Firestone curve is +-10% compared to the measurement of a real wheel.
    C. The material removal results of the simulation deviate utmost +-10% in comparison to the experiment.
    D. The energy consumption output for the rail grinding process is +-10% in comparison to the experiment.

    Challenges:

    A. To accurately model the grinding wheel topography is a challenging task because in the manufacturing process, the grain distribution on the wheel is stochastic. It's only possible to represent a grinding wheel that is statistically the same in the simulation,

not exactly the same. Thus, Abbott-Firestone is chosen as a matrix to represent the accuracy of grinding wheel topography modelling.

3. Deliverable 3: Optimized rail grinding process
    A. Optimized rail grinding process is achieved with 10% lower spindle power consumption and 2.5% lower total energy consumption.
4. Deliverable 4: Validation of the optimized rail grinding simulation in the lab
    A. The optimized rail grinding process found in the simulation is validated in the lab by achieving 10% lower spindle power consumption and 2.5% lower total energy consumption, which will remain in the range of +-10% material removal results compared to the non-optimized rail grinding process.
5. Deliverable 5: 5 field runs with Scheuchzer SA train to prove the energy saving measure:
    A. The energy consumption of the rail grinding process is predicted by 90% accuracy
    B. The spindle power consumption is decreased by 10% and the total energy consumption is decreased by 2.5%
6. Deliverable 6: Scaling up the energy-saving results to the entire rail grinding industry in Switzerland
    A. Define the scope of rail grinding in Switzerland where the optimized process can be applied.
    B. The annual energy saving potential reported in MWh

This report covers the results from work package 1 to 4, in other words, all deliverables from D1 to D4 are covered. The label of each deliverable is used throughout this report to indicate the relevant work done for the individual deliverables.

Description of facility

The initially planned project was split into three phases: simulation, lab validation and field validation. For each stage, various tools are appropriate to answer the research question: iBRUS software for simulation, Olga test bench for lab validation and Grizzly grinding train from Scheuchzer [10] for field validation.

1.4 iBRUS: The simulation software

iBRUS software is a simulation tool designed for simulating abrasive processes. It's designed in a modular way which makes it easily extendable and maintainable, as it's shown in Figure 5.

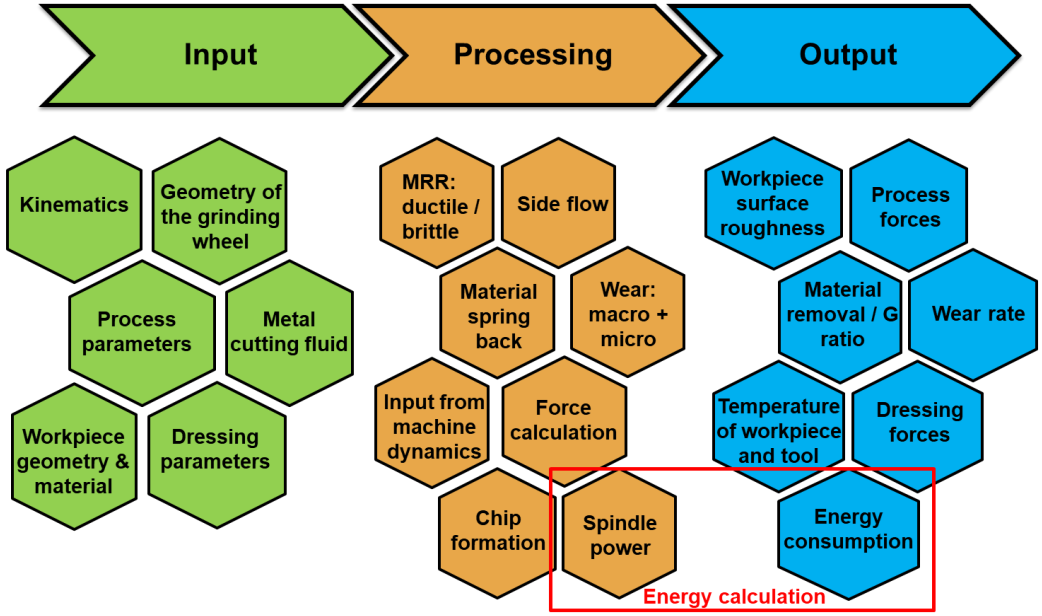

Figure 5 The modularity of iBRUS software

The simulation tool itself is a geometric-kinematic modelling tool that models the tool and workpiece interaction based on the geometric interactions of grains and workpiece planes, shown in Figure 6. The grains of the tool are 3D meshes as shown in purple, while the workpiece is a stack of 2D planes depicted in blue colour. The coordinate axes coloured with red, green and blue represent the position and orientation of the tool at each time step. After each of the time steps, the interactions of each grain with all workpiece planes are calculated according to the current and previous tool positions. Various physical simulation results are extracted through these interactions, such as tool force, tool wear, workpiece surface quality and material removal performance.

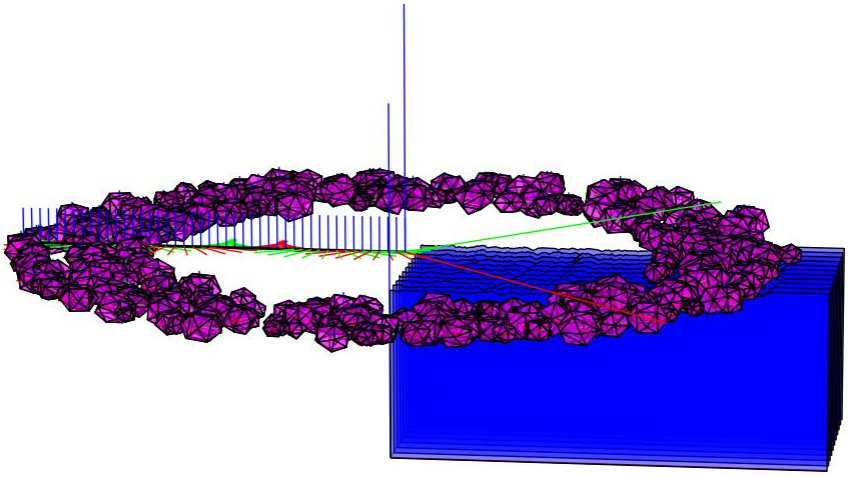

Figure 6 Representation of grinding process in iBRUS

1.5 Olga: The rail grinding test bench at inspire AG

The test bench at inspire AG for the rail grinding process is shown in Figure 7. It mainly consists of a vertical lathe, which provides a solid structure, a turntable and the necessary kinematics. The vertical lathe is equipped with a grinding unit on one side, the original turning tools and sensors on the other side and a ring-shaped rail steel workpiece on the turntable, as it's shown in Figure 7 and Appendix 10.1.1. The circular workpiece allows grinding at high feed rates for extended periods of time, which produces realistic thermal conditions. The test bench provides a controlled environment in which both in-process data and offline process data can be acquired using state-of-the-art sensors and measurement equipment.

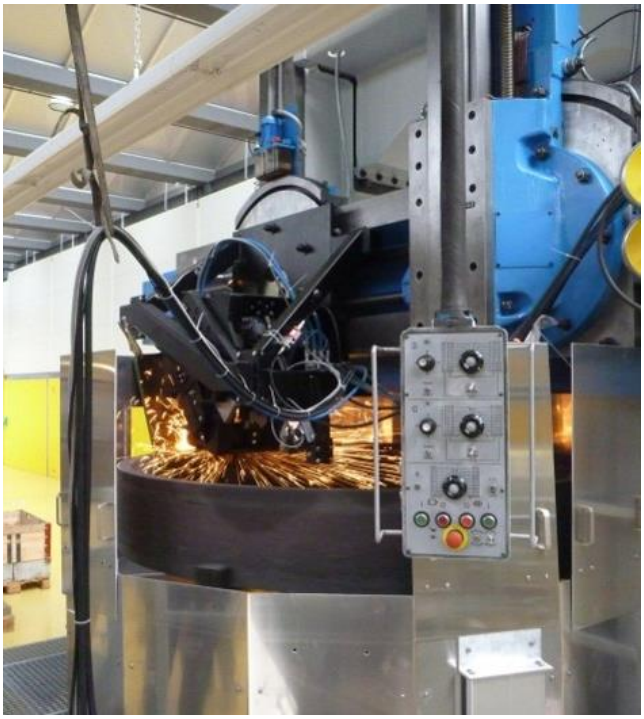

Figure 7 Picture of rail grinding test bench "Olga"

1.6 Grizzly: The grinding train

The field verification of optimal process parameters will be carried out by Scheuchzer. As an industrial expert, Scheuchzer has 7 different types of grinding trains, Grizzly series [10], that are capable of carrying out field testing. After the optimal process parameters are found in the lab environment, the industrial partner Scheuchzer will take the result of the experiment such as rotational speed and feed rate into the design of their operational parameter of Grizzly grinding train. An example picture of Grizzly grinding train is shown in Figure 8.

Figure 8 Example picture of Grizzly train.

2 Procedures and methodology

The general workflow of this project is to first realize rail grinding process and modules and predict energy consumption in the iBRUS tool. Then optimal rail grinding design or rail grinding operation parameters are searched by parameter studies. Once optimal parameters are found, validation should be carried out in the laboratory test bench.

In the work packages reported here, the focus is in three areas: 1) implement energy and temperature prediction model. 2) Validate the robustness of single grain scratch, by varying simulation parameters. 3) Implement rail grinding process models in iBRUS and calibrate and validate the rail grinding process against experimental results. 4) Optimize rail grinding process with the help of iBRUS simulation tool to get a 10 % lower energy consumption.

This report presents all the relevant results for rail grinding representation in iBRUS, energy prediction and optimization.

2.1 Robustness in material removal calculation: single grain scratch (D1.A)

The robustness of simulation is a measure of how stable the calculations are against the changes in process-specific or simulation-specific parameters. The response of simulation to the parameter changes should be predictable and stable, changing at a similar scale when process parameters are changed and converging to the real case when the resolution is increased by modifying the simulation parameters.

The single-grain scratch simulation is conducted to test the robustness of the iBRUS simulation. This simulation is performed with a grain from simple and known geometric shape and basic kinematics of translation or rotation. This way the real case result can be calculated analytically and compared to the simulation for robustness check.

Process-specific parameters control the physical objects and kinematics of the process; such as grain dimensions, tool size and feed-cutting speeds. On the other hand, simulation parameters do not influence the process itself but the resolution of the simulation. These are the workpiece plane spatial resolution (the distance between 2 planes) and the time step size of the simulation. As both of these parameters are set to finer values, the sensitivity of the simulation increases and the results approach ground truth, but the computational cost also increases with more planes and time steps. A balance is required between simulation accuracy and computational performance.

Overall, robustness analysis aims to:

- Ensure the results change as expected for a range of process parameters, so different sets of parameters can be tested to observe process behaviour
- Find the ranges of simulation parameters giving an acceptable margin of error and runtime

2.2 Implementation of the temperature and energy models (D1.B)

2.2.1 Temperature Model

The iBRUS software is a grain-based simulation tool, which gives the possibility to investigate temperature rises at the grain level. For the temperature model Takazawa [14] temperature model is adapted from using tool-based parameters to using grain-based parameters.

Takazawa [14] gives a tool-based equation to approximate the maximum temperature rise at the cutting surface by assuming grains as moving ideal heat sources, which was simplified by Kato and Fuji [15] as:

$$\theta_s = 3.1 \frac{2R_w q\alpha}{\pi k V_w} \left(\frac{V_w l}{2\alpha}\right)^{0.53} \tag{1}$$

$$\theta_m = \theta_s \exp(-\beta z) \tag{2}$$

$$\beta = 0.69 \left(\frac{V_w l}{2\alpha}\right)^{-0.37} \frac{V_w}{2\alpha} \tag{3}$$

θ_m: $maximum\ temperature\ rise\ at\ a\ given\ depth$

θ_s: $maximum\ temperature\ rise\ at\ the\ surface$

l: $half\ length\ of\ band\ source$

l_c: $contact\ length\ bewteen\ wheel\ and\ work$
q: $heat\ flux\ (\ heat\ generated\ per\ unit\ area) = F_t V_s/(l_c b)$
R_w: $energy\ partition\ coefficient$
V_S: $wheel\ speed$

V_w: $workpiece\ speed$

β: $coefficient$

α: $thermal\ diffusivity\ of\ workpiece\ \left(=\frac{k}{\rho C}\right)$

ρ: $density\ of\ workpiece.$

C: $specific\ heat\ of\ the\ workpiece.$

k: $thermal\ conductivity\ of\ the\ workpiece$

The energy partition ratio R_w should not be confused with the ratio between total cutting power and total power input. The R_w is defined as the proportion of the grinding energy conducted into the workpiece in the contact area, according to Rowe [16].

For the rail material, some of the thermal properties are already known, as listed in the following table, is taken from Kuffa [17]

Thermal conductivity (k) [W/mK]	38
Specific heat capacity [J/kgK]	477
Melting point [K]	1793
Reference temperature [K]	293
Density [kg/m3]	7830

Table 1 Thermal properties of rail material [17].

The total energy input of the grinding process is transformed into different parts. In the work of Aggarwal et al. [11], the total electrical power consumption of the spindle is predicted from the spindle current with estimations for all types of losses, as it's shown in Equation (4).

2.2.2 Energy Model

$$UI = P_E = P_{cut} + P_{ml} + P_{el} = M\omega + P_{ml} + P_{el} \quad (4)$$

Where P_E is the electrical power, P_{cut} is the cutting power, P_{ml} is the mechanical power loos, P_{el} is the electrical power loss, M is the grinding wheel torque and ω is the rotational speed of the grinding wheel.

The key challenge is to quantify how much of the total power goes into the cutting power. One approach is to measure and quantify the energy that is consumed by separate system, such as spindle motor, cooling unit, etc. For example, as it's shown by Aggarwal et al. [11], total energy consumption is quantified in separate parts shown in Figure 9.

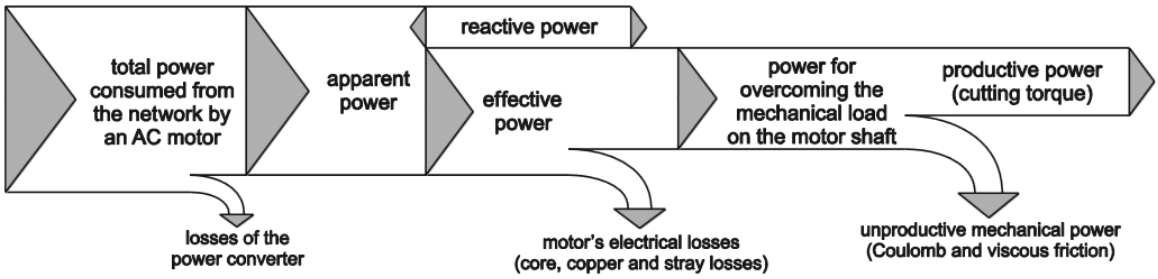

Figure 9 Power flow in a motorized spindle [10]

The optimization of this area mainly concerns optimizing the energy transition efficiency from the power grid to the spindle. The solution to these will be largely limited to rail grinding setup, which will be hard to scale and are not the focus of this project. The focus of this project will only be on the power used by the spindle for cutting.

According to M.C Shaw [12] and Malkin [13], P_{cut} in Equation (4), essentially all energy spent in cutting is dissipated as heat. Then the total amount of heat is dissipated into the workpiece and grains by conduction and into chips and cutting fluid by convection. Rail grinding requires high energy because of its dry grinding nature and high material removal rate demand, which could cause thermal damage such as grinding workpiece surface burns [13]. One of the challenges in achieving a higher material removal rate is to avoid thermal damage. Thus, a temperature model is needed to indicate when the workpiece surface reaches a dangerous temperature that can cause workpiece burn.

Weerasekara [18] implemented a grinding energy model using the discrete element modelling (DEM) technique, by solving Newton's motion equation to resolve particle motion and using a contact law to calculate force and energy dissipation during the process. Singh et al.[19] used various models to quantify the energy dissipation in three phases: ploughing, chipping, secondary rubbing, and primary rubbing. However, it requires accurate division between several phases of grinding in the simulation. The approach used in this project is based on a geometric and kinematic simulation tool that doesn't differentiate the various phases of grinding.

For the first step of calculating energy, the following equation is used for each grain to get grain-based grinding energy, P_{cut} in Equation (1) then can be calculated as the total sum of all grinding energy for each grain as shown in Equation (2)

$$P_{cut} = \sum_{i=1}^{N} F_{c,i} \omega R \tag{2}$$

$F_{c,i}$ is the cutting force for each grain. ω is the rotational speed of the wheel and R average grinding wheel radius.

2.3 Rail grinding process implementation in iBRUS

2.3.1 Rail grinding tool modelling in iBRUS (D2.B)

Gharaei et al.[23] elaborated on the virtual grinding wheel creation methodology where it is used to create two virtual rail grinding wheels of grain size A16 and A8 that are resembling the actual one. This

report assumes the same methodology and elaborates on the A16 virtual grinding wheel generation in the following.

The following assumptions have been taken for the creation of the grinding wheel:

1) Cuboctahedron represents the grains in grinding wheel.
2) Grains are different in size and can be described by a normal distribution characterized by the mean and standard deviation of grain volumes.
3) The grinding wheel's grain density is uniform across different regions of the grinding wheel. Therefore, the virtual grain's position and orientation in the tool are specified with a uniform random distribution.

The grains material ratio of the actual wheel is also required to define the number of virtual grains to be distributed in a cylindrical spatial form. The actual grinding wheel's cross-sectional image analysis shows a 60% grain material ratio approximation – see Figure 10. The 40% remaining ratio corresponds to the bonding and pores.

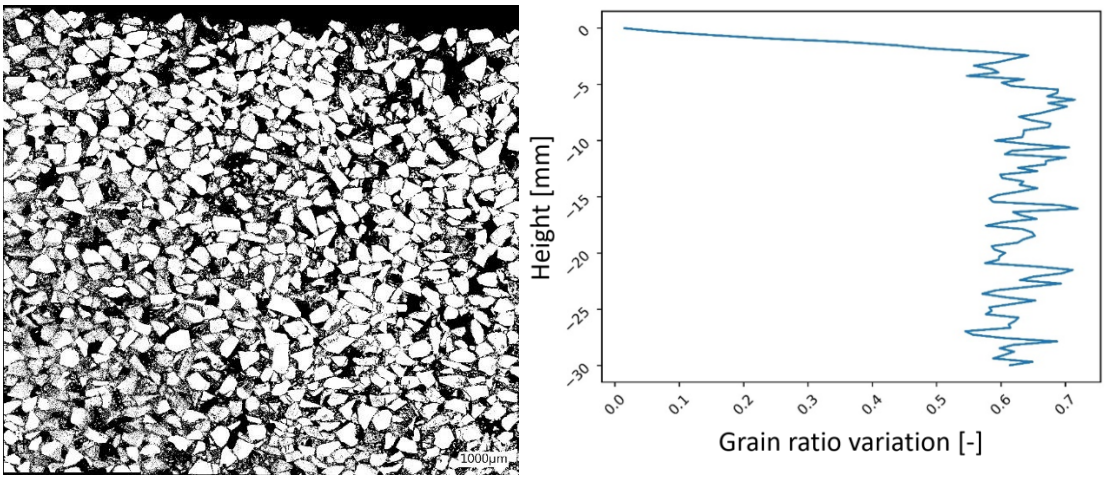

Figure 10 Left image: an image of a cross-sectional cut captured by a Keyence digital microscope. Right image: grain ratio variation along the wheel's height observed in the left image.

Typically, grain size distribution is provided by the wheel manufacturer. In the absence of such information, as is the case for this report, the normal distribution parameters (mean grains volume and standard deviation) must be defined. The standard mesh size of 16 for the A16 wheel type, does not physically allow a cuboctahedron with a volume of more than $3.3\ mm^3$ pass through. Parameter-set candidates shall be selected in a way that the chance for the presence of a grain with a bigger size is rare. Therefore, three distribution parameter sets are assumed, as it's shown in Figure 11. As can be seen, the statistical parameters are chosen in a way where the chance of grain more than this limitation is 0.001%. In the case of $N(\mu = 1.7\,, \sigma = 0.38)$ grains are assumed to be more variant in size compared to the scenario where $N(\mu = 2.1\,, \sigma = 0.28)$. For each hypothesized grains distribution, a virtual grinding wheel is generated. Such variation in the wheel's grain size distribution leads to the generation of grinding wheels with distinctive topographies at their grinding surface. Finally, the topography of the virtual wheel candidates is compared to the actual wheel topography and the closest is picked.

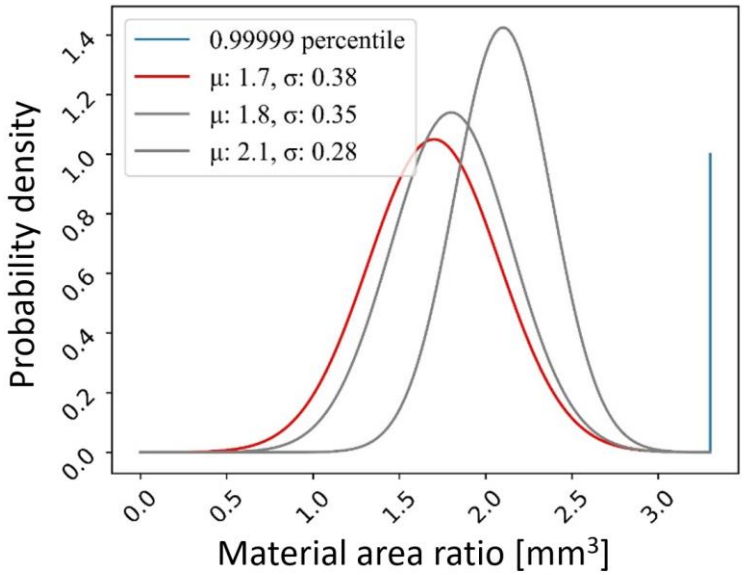

Figure 11 Three hypothesized normal distributions for the grains size distribution of the A16 wheel.

2.3.2 Material removal volume in rail grinding simulation (D2.C)

Material removal results from experiment are calculated as shown in Equation (5). The depth of cut a_p is a measurement result of a rail grinding experiment. After a_p is obtained, the removed volume could be easily calculated for each rail grinding experiment. This equation is derived based on the Olga test bench setup illustrated in Figure 12.

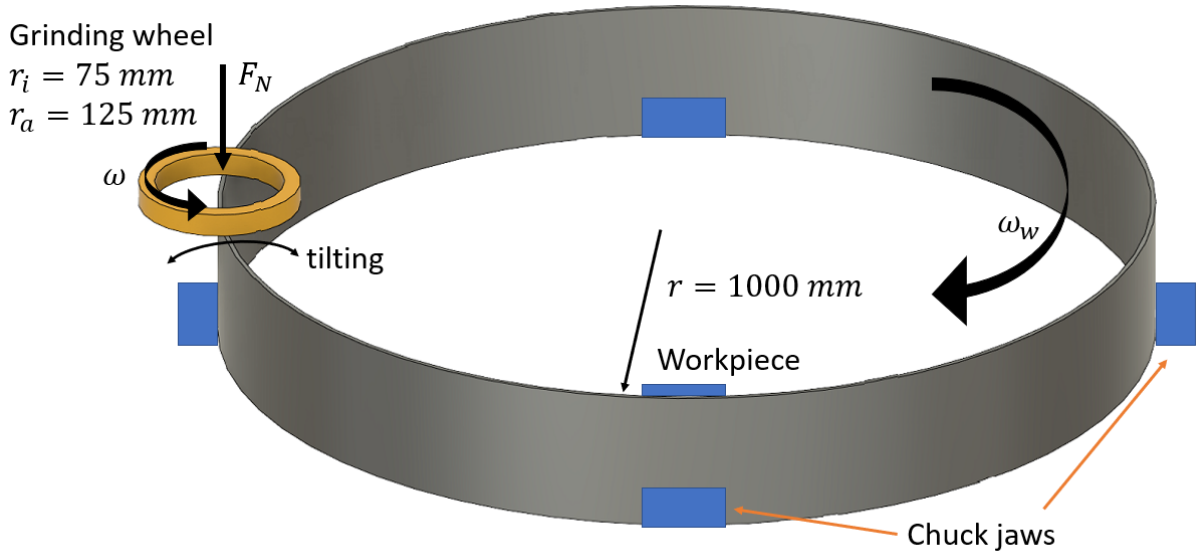

Figure 12: Illustration of experimental setup for rail grinding on Olga

$$V_{exp} = a_p W_W \omega_w r t \tag{5}$$

Where W_W is the facade with of the workpiece ring, ω_w is the rotational speed of the workpiece ring in radiant/s, r is the radius of the workpiece ring t is the grinding time.

The material removal calculation in the iBRUS simulation is based on a grain and plane interaction model. By default, the material removal model (MRM) implies an ideal cut with a simplified Boolean form of material removal. Thus, no material deformation or ploughing is assumed. The MRM is used to calculate material removed by each grain based on the geometrical intersections between individual grains and workpiece planes. The result of such calculations from MRM is then available for the other models such as force model.

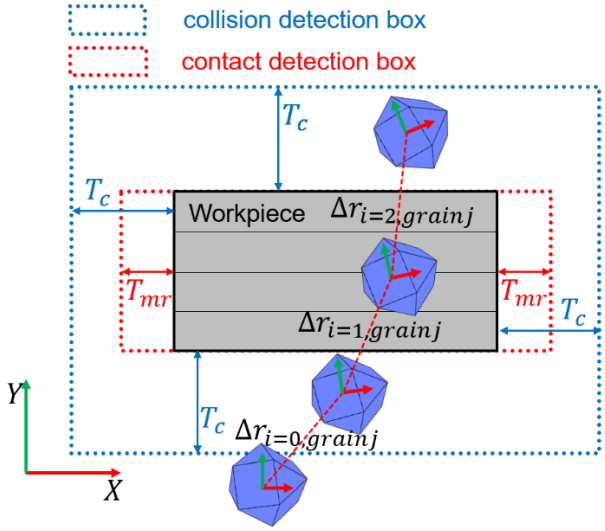

Figure 13 Simplistic representation of MRM in iBRUS

The material removal model in iBRUS is shown in Figure 13. The very first phase of the MRM is to determine if grains are in close proximity to the workpiece volume. T_c represents a distance-based collision detection threshold. In any simulation time step, any grain which is out of collision detection box enclosed by collision detection threshold is not considered for material removal calculation. T_{mr} represents contact detection threshold. Any grain that is out of the contact detection box within any simulation step will not remove volume. Checking for these two proximities yields more accurate calculations and greater simulation efficiency by eliminating unnecessary calculations.

For every grain in workpiece proximity, then, it is determined whether it has traversed any of the workpiece planes. The material removed by every grain is calculated based on the grain's travelled distance and the projected cutting area it leaves on the workpiece planes along its path between the current simulation step and last simulation step. The position of the grains at each simulation step is known. Therefore, every grain's traveling direction and distance, shown as Δr_i in Figure 13, are calculated based on the grain's position between two consecutive simulation steps. The grain's projected cutting area on each plane is also calculated through the projection of the grain's 3D mesh onto the 2D workpiece plane. Finally, a grain's overall removed volume between two simulation steps comes from the sum of the multiplication of the projected areas with the grain's orthogonal displacement to the areas.

In order to fulfil deliverable D2.C, the calculated removed volume from experiment, V_{exp} from Equation (5) is used as a comparison baseline to compare against V_{sim}. The deviation of V_{sim} and V_{exp} should not differ more than 10% to meet deliverable D2.C.

2.3.3 Efficient rail grinding simulation (D2.A)

The computational efficiency of the simulation tool is an important aspect in simulation software development. Because in the realistic use case, the optimization of the process will require several iterations, thus the time for one simulation run needs to be reasonably short, which is determined as 1 hour for 0.1 seconds of real process time in the deliverable D2.A.

To reach this deliverable, a benchmark case is defined, shown in Figure 14. In this case, at the start of the grinding process, the grinding wheel is positioned at the side of the workpiece at a certain height. This tool height is calculated to get an average depth of cut around 7 μm as it moves towards the workpiece and rotates around its z-axis.

For general simulation parameters: the number of workpiece planes chosen for this simulation is five and simulation step size is 360 steps per tool revolution.

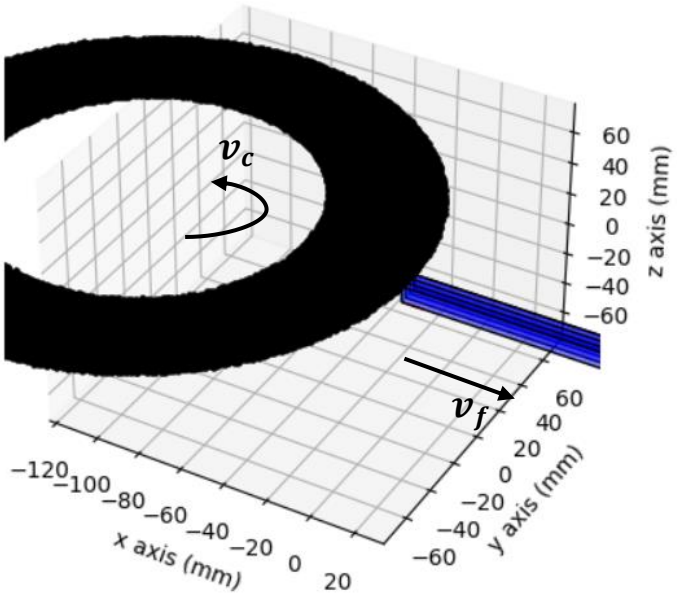

Figure 14: Starting position and kinematics of rail grinding efficiency simulation

2.4 Energy consumption prediction using iBRUS (D2.D)

2.4.1 Definition of the scope of feasible process parameters

The foundation of energy consumption simulation is to define a realistic range of process parameters. This enables simulations to accurately represent real-world scenarios and serves as a basis for further optimization. Defining a parameter range also ensures that any optimization measures obtained will be likely practical to implement in the field.

In the case of the rail grinding process, which is a force-controlled process, there are three fundamental process parameters: normal force, feed rate of the workpiece, and cutting speed of the tool. The normal force is measured directly using force (N), while the cutting speed of the tool is

determined by the frequency of the spindle rotation (Hz). As the grinding unit on Olga and the Scheuchzer train are similar, the rotational speed of the spindle can be directly applied in the field. The feed rate of the workpiece is measured differently on Olga and on the train. The workpiece on the test bench takes the shape of a workpiece ring, and its feed rate is measured by the rotational speed of the workpiece ring (RPM). When applying the same feed rate on the grinding train, it needs to be converted into the linear speed of the workpiece ring, which has a radius of 1 meter.

In the following chapters, experimental results will be presented using workpiece rotational speed [RPM] and spindle frequency [Hz], while simulation results will be presented using feed speed [mm/s] and spindle frequency [Hz], since the simulation in iBRUS mimics the kinematics of the grinding train, not Olga.

Based on the grinding experience at IWF and the reliability of the experimental setup, a range of parameter that gives the most confident results are chosen, as it's shown in Table 2.

Process Parameters	Feasible Parameter Range				
Normal force [N]	1400	1600			
Spindle frequency [Hz]	40	50	60		
Workpiece rotational speed [RPM]	10	12.5	16	20	25

Table 2 Scope of experimental process parameter range

Under the same normal force, the feasible feed rate and cutting speed composes a 2-dimensional matrix, shown as a table, which will be used throughout this report to showcase experimental and simulation results.

Since the parameter chosen in Table 2 is a set of process parameter that gives the most reliable experimental data, it only represents the data range where a confident mathematical model and simulation can be built. It's important to note that other combinations of process parameters, not shown in Table 2, are also feasible to be executed on the Olga test bench. When considering optimization, the process parameter choice will not be limited to Table 2.

2.4.2 Experimental data collection

According to the feasible range of process parameters defined in 2.4.1, two sets of experimental data need to be collected. One set at 1400 N normal force, the other at 1600 N normal force. Collection of these data sets should give the possibility of investigating the relationship between a_p and v_f, v_c under the same F_n, as well as the relationship between F_n and a_p under the same v_f and v_c.

The first set of experimental data, which includes Exp 560, Exp 561, Exp 564 and Exp 566, was collected in a parameter study where the parameters feed rate (v_f) and cutting speed (v_c). have been varied, achieving different cutting depths (a_p) and consequently material removal rates (Q). The parameter sets used in the experiments can be taken from Table 3. After a warmup grinding cycle to sharpen the grinding tool and reach desired tool sharpness, 180 seconds long grinding cycles are used for data acquisition. A quasi-static state is reached where cutting depth and process forces are steady. From the quasi-static phase of the experiment, friction coefficient μ, depth of cut a_p and the normal force F_N are extracted and used to calibrate the simulation and build models to predict a_p based on feed and cutting speed.

The second set of the experiment is conducted for the optimization research for RESI projects. This set includes Exp 587, Exp 590, and Exp 592. Except Exp 587 is conducted with the normal force of 1400 N, the other two experiments are conducted with a normal force aiming 1600 N.

		Spindle frequency		
		40 Hz	50 Hz	60 Hz
Feed speed	10 RPM	Exp 587		
	16 RPM	Exp 566	Exp 561	Exp 560 Exp 590
	25 RPM			Exp 564 Exp 592

Table 3: Experiment sets conducted

2.4.3 Calibration of iBRUS

In order to get accurate energy consumption results out of iBRUS, the simulation input parameters must be calibrated so that the simulation results represent experimental results. The challenge lies in the distinction between the grinding processes employed on the grinding train and the Olga test bench, both of which are force-controlled. On the other hand, iBRUS utilizes a predefined path, rendering it path-controlled. This disparity gives rise to a disparity in input parameters and outcomes between the simulation and the experiment. As a result, aligning these differing methodologies becomes a critical concern. While in the experiment the normal force is an input, in simulation the normal force is an output. Other way around, in the simulation, the depth of cut is an input while in the experiment it is an output. The relationships for experiments and simulations are shown in Equation (6) for experiment and Equation (7) for the simulation.

$$a_{p,exp} = f(F_{N,exp}) \tag{6}$$

$$F_{N,sim} = f(a_{p,sim}) \tag{7}$$

To bridge the gap between experiment and simulation, the strategy used to calibrate the simulation involves a two-step process. In the first step, the tool height set position for simulation is found, so that resulting depth of cut is the same for the experiment and the simulation. In the second step, the specific cutting force k_c is adjusted so that the normal force of the simulation matches the resulting normal force of the experiment.

The purpose of using iBRUS simulation is to save the time and material cost for the preparation and execution of experiment. To be able to do that, iBRUS needs to be able to simulate all combinations of cutting speed and feed speed.

To simulate combinations of feed and cutting speed where there are no experimental results, a mathematical model must be established to predict depth of cut for the same set of normal force. This is done by first calculating the percentage decrease from depth of cut of Exp 560 to Exp 564. This result will give some percentage decrease of depth of cut for a feed speed increase of 9 rpm. With that information, the missing cells for 25 rpm are calculated, indicated in red in Table 4. Since there are now two depths of cut for each spindle frequency, the linear regressions for a shift in feed speed can

be done. With the results of these regressions, all other missing cells can be calculated, indicated in green. The results can be seen in Appendix 10.3.1.

		Spindle frequency		
		40 Hz	50 Hz	60 Hz
Feed speed	10 RPM	$A_{p,(10,40)}$	$A_{p,(10,50)}$	$A_{p,(10,60)}$
	12.5 RPM	$A_{p,(12.5,40)}$	$A_{p,(12.5,50)}$	$A_{p,(12.5,60)}$
	16 RPM	$A_{p,16,40}$ (Exp 566)	$A_{p,16,50}$ (Exp 561)	$A_{p,16,60}$ (Exp 560)
	20 RPM	$A_{p,(20,40)}$	$A_{p,(20,50)}$	$A_{p,(20,60)}$
	25 RPM	$A_{p,(25,40)}$	$A_{p,(25,50)}$	$A_{p,(25,60)}$ (Exp 564)

Table 4: Experiments used for depth of cut model

With the depth of cut calibrated, the normal force now must be calibrated. In Equation (8) it is shown how the tool normal force for simulation step j $F_{N,j,tool}$ is calculated in the simulation.

$$F_{N,j,tool} = \sum_{i=0}^{N} \frac{F_{C,i}}{\mu} = \sum_{i=0}^{N} \frac{k_c A_{cut,i}}{\mu} \tag{8}$$

Where N is the number of grains in the tool, $F_{C,i}$ is the cutting force of grain i and $A_{cut,i}$ is the projected cutting area of grain i.

Since $A_{cut,i}$ and μ are fixed, the only variable that can be changed is k_c. The specific cutting force is then adjusted so that the normal force has the same value for both the simulation and the experiment.

2.4.4 iBRUS simulation and prediction of energy

Simulations are conducted in the range of defined parameters in Section 2.4.1. Since the simulation is calibrated on the parameters in the quasi-static state, the length of simulation doesn't need to correspond to experiment, so long as removed volume comparison is not the goal. Hence in this case, shorter simulations are conducted.

To compare the results between experiment and simulation that have different time length, specific energy consumption, which is defined as energy consumption per volume removed is calculated as energy efficiency parameter for the experiment and simulation, using Equation (9) and Equation (10).

$$E_{sim} = Pt = F_c \omega R t = \omega R t \frac{1}{T} \sum_{j=1}^{T} \sum_{i=1}^{N} k_c A_{cut,i,j} \tag{9}$$

$$\frac{E_{sim}}{V_{sim}} = \frac{Pt}{a_p v_f t W_W} = \frac{F_c \omega R t}{a_p v_f W_w t} = \frac{F_c \omega R}{a_p v_f W_W} = \frac{\omega R \frac{1}{T} \sum_{j=1}^{T} \sum_{i=1}^{N} k_c A_{cut,i,j}}{a_p v_f W_w}$$

(10)

In Equation (9), the spindle rotational speed ω and grinding wheel average radius R are known inputs to the simulation. $A_{cut,i,j}$ is the cutting area of grain i at the simulation step j, which is a result of simulation at each simulation step. T is the total number of simulation steps. The value of k_c comes from calibration process, which produce the same normal force when performing under cutting speed and feed speed.

2.5 Energy consumption optimization (D3.A)

The target of optimization is to find a set of process parameters, which includes normal force, cutting speed (spindle frequency) and feed speed, which in turn yields optimal energy efficiency. In other words, a set of F_N, ω and V_f that minimize the Equation (11). In this equation, energy efficiency is defined as the amount of energy consumption per volume of material removed, called specific energy consumption.

$$\frac{E_{exp}}{V_{exp}} = \frac{Pt}{a_p v_f t W_W} = \frac{F_c \omega R t}{a_p v_f W_w t} = \frac{F_N \mu \omega R}{a_p v_f W_W}$$

(11)

An ideal case can be found when experimental data are available for all combinations of F_N, ω, v_f, which results in a three-dimensional matrix. An exhaustive search in this three-dimensional matrix would yield the target process parameters.

The exhaustive search in this three-dimensional matrix requires sufficient data from experiment and trustworthy models. However, an exhaustive set of experiments is time and cost intensive. In addition, the uncertainty and variability of experiments makes the acquisition of good data difficult. Thus, simulation results will be used once the simulation of rail grinding process is validated. Based on the collected data from experiment and simulation, a mathematical model could be built to discover the relationship between $\frac{E_{exp}}{V_{exp}}$, v_f and ω. This discrepancy warrants further investigation in the future to ascertain its significance and implications.

The biggest challenge to explicitly describe the relationship between $\frac{E_{exp}}{V_{exp}}$, v_f and ω is two sets of $v_f \sim a_p$ and $\omega \sim a_p$. When both v_f and ω are changing in Equation (11), a_p will also change. With an appropriate model and an according simulation, the point can be estimated. Thus, the discovery of the optimal point of $\frac{E_{exp}}{V_{exp}}$ can only be discovered empirically. With the modelling and simulation technique, the direction in which one has to go, can be estimated and therefore less experiments have to be performed. With more and also very specific experiments, the model could be designed in a way that it can predict energy consumption very precisely.

3 Results and Discussion

3.1 Single-grain scratch simulation to test the robustness of iBRUS

A single-grain scratch simulation has been conducted to test the robustness of the simulation by varying simulation step size and the number of workpiece planes. The process of this simulation is shown in the Figure 15. The process parameters used in this simulation are sampled from a setup of rail grinding parameters, which are shown in Table 5.

Rotational speed [rpm]	3600
Feed rate [m/s]	0
Workpiece dimension x [mm]:	100
Workpiece dimension y [mm]:	10
Workpiece dimension z [mm]:	30
Number of grains in tool [#]	1
Grain shape	Cube mesh
Grain size (side length) [mm]	1.732
Radius of single grain tool	75
Cutting area [μm^2]	80

Table 5 Process parameters used in single grain scratch simulation

Two parameters were chosen to vary for robustness analysis: the number of workpiece planes and simulation step size. The number of workpiece planes represents the resolution of workpiece as illustrated in the Appendix 10.1. The simulation step size represents the resolution of the entire simulation and is measured in steps per revolution of the grinding wheel.

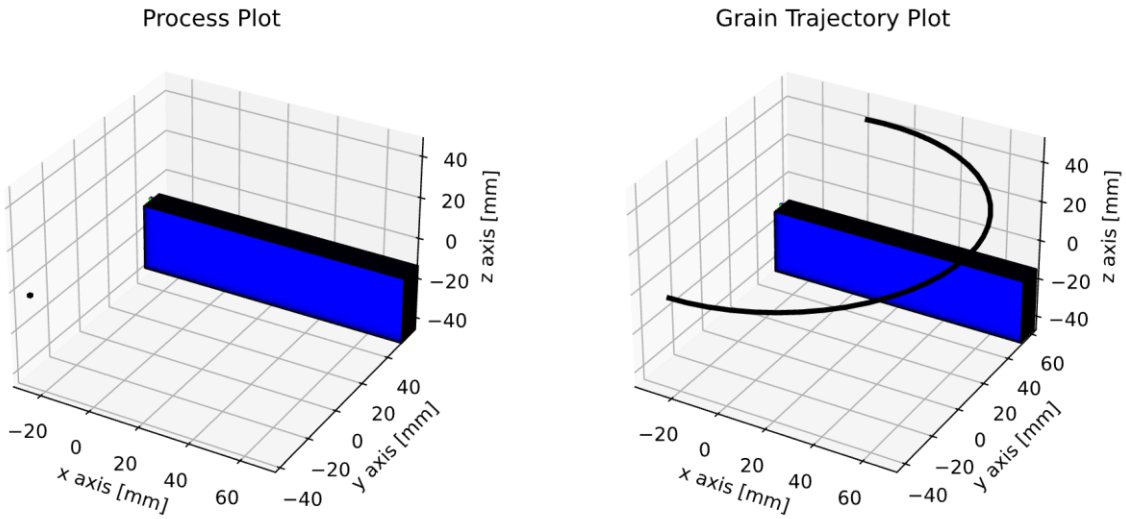

Figure 15 Visualization of single grains scratch. (On the left: plots of one cubic grain and workpiece. On the right: plot of grain trajectory going through the workpiece)

The results of material removal percentage deviation from simulation to analytically calculated are shown in Figure 16 and Figure 17, respectively, in the cases when simulation step size and number of workpiece planes are varied.

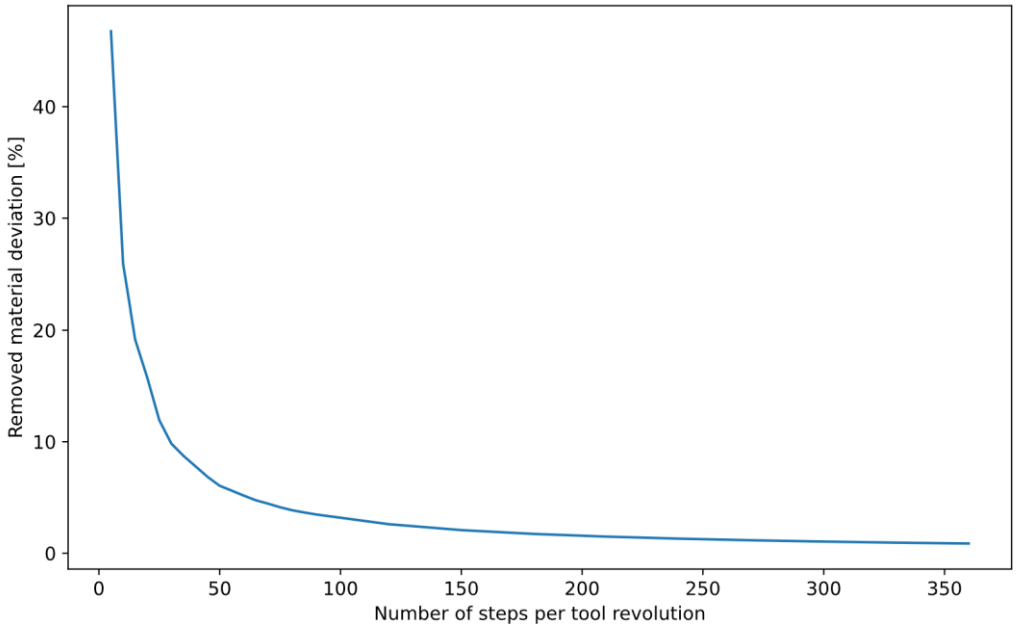

Figure 16 Removed material sensitivity against simulation step size

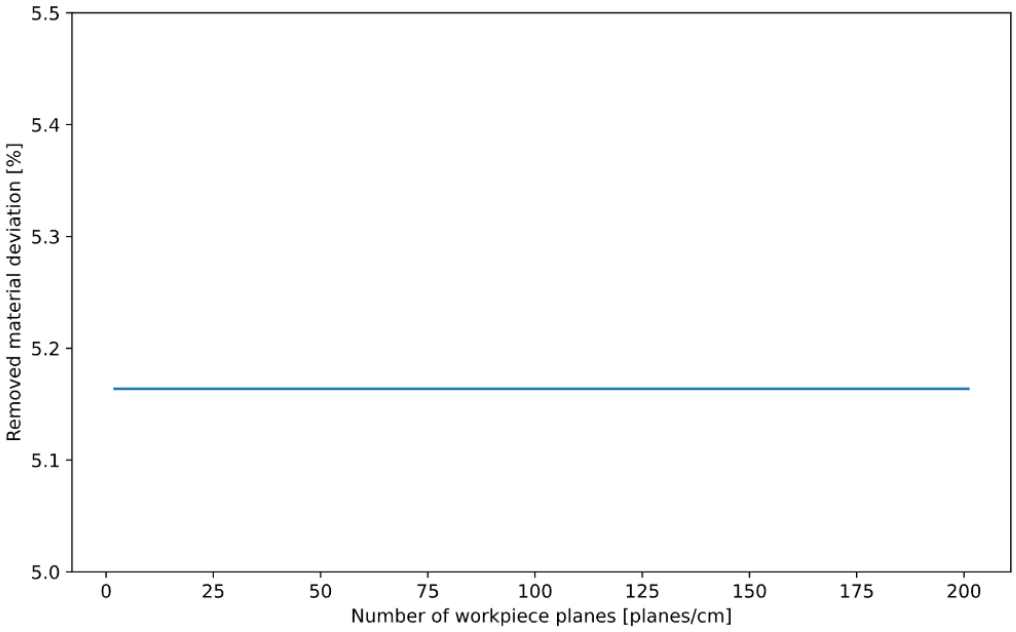

Figure 17 Removed material sensitivity against the number of workpiece planes

3.2 Temperature and Energy Model

The temperature and energy models are applied in the same single-grain scratch simulation that is used for the robustness analysis. The results of the temperature rise of the grains are shown in Figure 18.

Since it is a single-grain scratch simulation, where the grain passes the workpiece once, the maximum amount of heat is naturally shown as a pulse, which represents the period when grinding is happening.

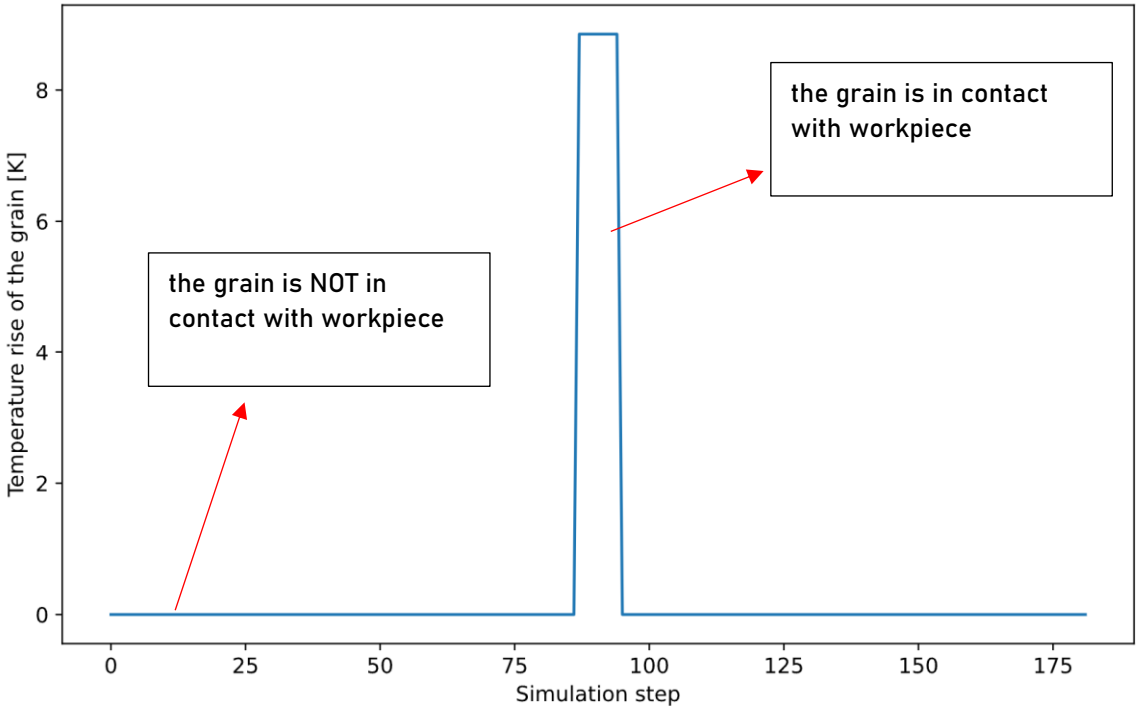

Figure 18 Temperature rise of single grain scratch simulation

The result of the energy model of a single-grain scratch is shown Figure 19.

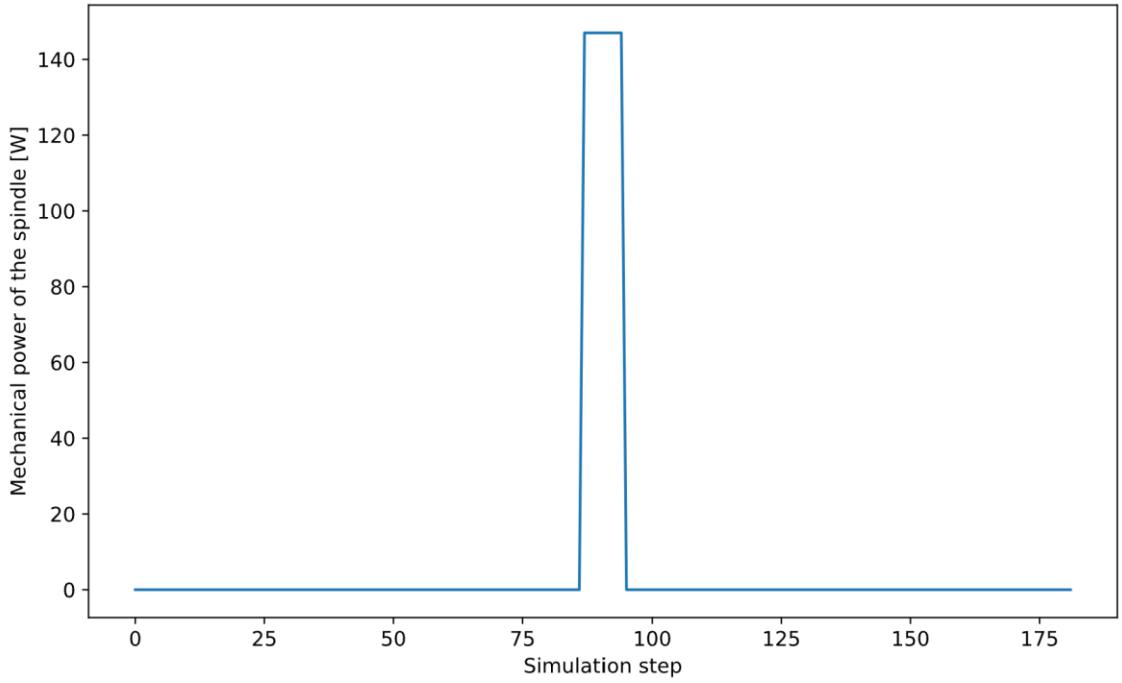

Figure 19 Energy model results; mechanical power of imaginary spindle with one single grain

3.3 Representing rail grinding process in iBRUS

3.3.1 Result of grinding wheel topology representation

The Abbott-Firestone curve is widely used for topography characterization. It is used here to evaluate the generated virtual grinding wheels by comparing their topographies against the experimentally measured grinding wheel topography.

The material ratio of the actual wheel was obtained from a linearly-trend-adjusted primary profile, which was recorded with a scanCONTROL LLT3060-50/BL laser profile sensor from Micro-Epsilon. The measurement corresponds to a 30.0 mm long distance in the radial direction on the cutting surface of the grinding wheel where the distance between two measurement points is 1 µm. To select the best virtual wheel candidate, the virtual grinding wheel's grain ratio is compared to the measured actual wheel's material ratio curve, as shown in Figure 20. The figure illustrates both the Abbot Firestone curves for the virtual wheels and the actual wheel.

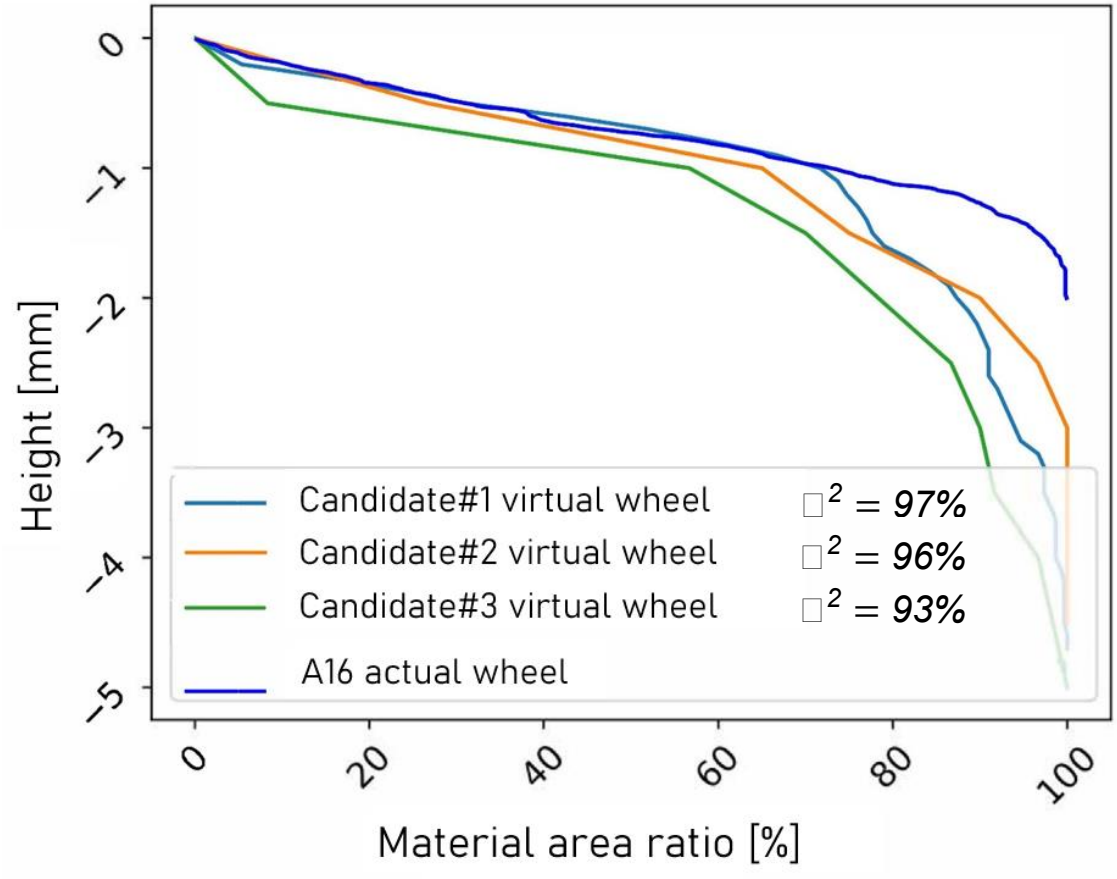

Figure 20 Derived Abbott-Firestone curves for the actual as well as the virtual wheel candidates generated based on the three hypothesized size distributions; candidate#1: N(µ=1.7 ,σ=0.38), candidate#2: N(µ=1.8 ,σ=0.35), and candidate#3: N(µ=2.1 ,σ=0.28) (Gharaei et al [20])

As can be seen in Figure 20, Candidate #1 shows the greatest recognizable similarity to the measured topography and is therefore used for the further course of the investigation, even if none of the candidates fully corresponds to it. The discrepancy, especially at the right-hand end of the Abbott-Firestone curve (100% material content), can be explained by the fundamental difference between

simulation and experimental topography measurements: In the experimental measurement, the binding is included in the Abbott-Firestone curve, though this is not relevant for the material removal. In the simulation the absence of virtual binding causes deviation of the simulation Abbott-Firestone curves from nearly -0.6 mm or lower. Such difference does not play a major role since the cutting happens by the most protruded grains that the left side of the curve represents. The left half of the curve is therefore used as an indicator for the validation of the generated simulation grinding wheels.

3.3.1 Result of material removal comparing to experiment

To compare the simulated removed volume and experimental removed volume, a simulation is conducted to represent 1 second of a rail grinding experiment. The overall results comparing the removed volume is shown in Table 6. As it demonstrates, the simulated removed volume overall is only 2.94% more than the experimental results. The deliverable target, D2.B, was set at 10% deviation. Thus, this deliverable is met.

	Experimental Result	Simulation Result	Deviation
Removed volume [mm3]	131.36	135.22	2.94%

Table 6 Removed volume comparison between experiment and simulation. (D2.B)

The experimental result presented in this table is calculated based on the workpiece dimension, feed rate of workpiece and the resulting depth of cut as it is shown in Equation (5). The result from simulation comes from the direct output of simulation.

3.3.2 Runtime performance of rail grinding simulation

The number of grains in the grinding tool for this deliverable is determined as 20,000. In a realistic wheel 20,000 grains would correspond to multiple layers of grains, some of which may not interact with the workpiece in this benchmark case. The grain number to fill one layer in this benchmark case is around 13300. The grains not interacting with the workpiece do not change the results but affect the computational effort, so they can be ignored with no adverse effect to this case.

Still, to comply with the initially set deliverable, a different grinding wheel with smaller grains to get 20,000 grains in one layer is created, then both 13300 grain and 20,000-grain wheels are tested for runtime.

In the end, the runtime for the 13,300-grain wheel was 3,300 seconds (~55 minutes), and for 20,000-grain wheel was 3,560 seconds (~59 minutes). Thus, the desired runtime of under 1 hour is achieved for both cases.

The result for this benchmark is also robust, since the chosen simulation step size and number of workpiece planes, which are 360 steps per revolution and 5 workpiece planes, respectively, produce minimal material removal deviation, according to results presented in the section 3.1.

3.4 Energy consumption prediction

3.4.1 Experimental results collection

When conducting experiments, continuous measurement data is read out from the entire process of grinding. However, for calibration of the simulation tool, only one number is extracted per variable from the experiments. So when raw experimental data is collected, a two-step data processing flow is adapted to generate the results shown in Figure 21, Figure 22, Figure 23 and Table 7. The two-step data processing flow is described in detail in the Appendix 10.2.1.

In the tables below one can see the results from the experiments performed on the Olga test bench at inspire AG. The results included the depth of cut a_p, the normal force F_N and the friction coefficient μ.

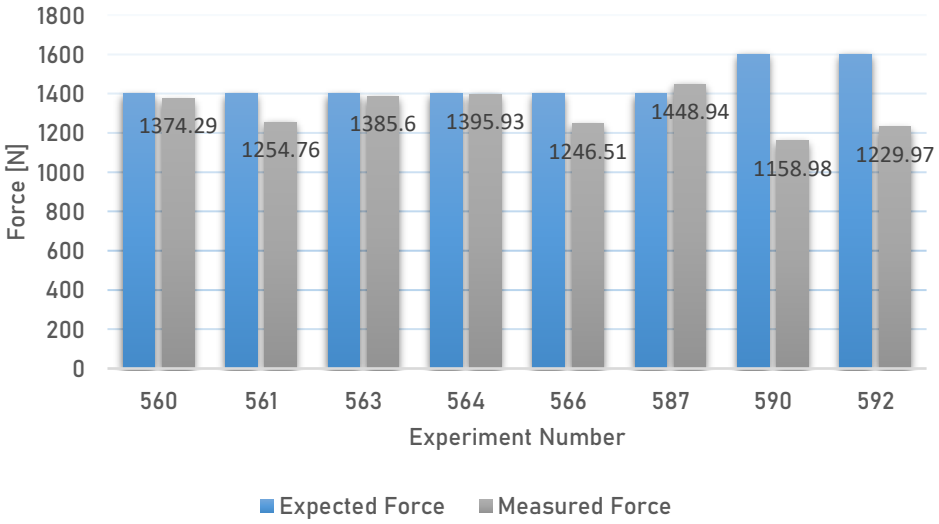

Figure 21 Controlled force versus measured force results from experiments.

Figure 21 shows controlled forces, measured force results, and the difference between them. As it can be seen, the difference between the controlled force and measured force result is highest in Exp 590 and 592. The reasons for this are due to the uncertainty in the experimental control. See section 4.5 for a detailed discussion.

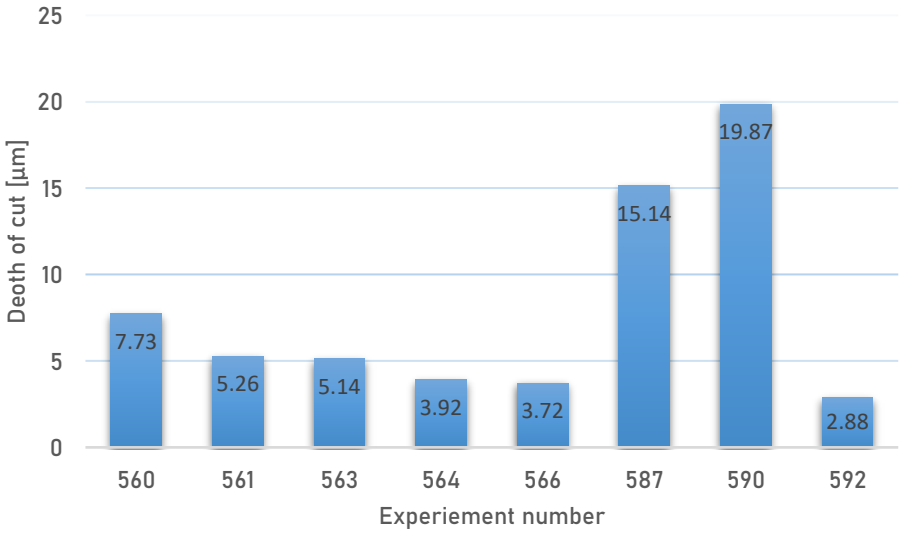

Figure 22 Depth of cut results from experiments.

In Figure 22, the measured depth of cut of all experiments are shown. It's obvious that Exp 587 and Exp 590, show unproportionally large depth of cut, comparing to the other experimental results. For example, comparing depth of cut from Exp 587 and Exp 566, the experimental data is extracted when the tool state is roughly the same. Comparing to Exp 566, the Exp 587 measured 16.7% higher force and 37.5% lower feed speed, but the depth of cut is 3 times higher. This is a strong contrast when comparing Exp 560 to Exp 564, where the Exp 560 has also 36% lower feed speed comparing to Exp 564, but the depth of cut is only 1 time higher than Exp 564. The similar abnormality is also observed when comparing Exp 590 to Exp 592.

The main reasons for unproportionally high depth of cut is mainly due to different tool state. Although the friction coefficients are very close, the tool profile might be vastly different. See more detailed discussion in Section 4.5 Based on this comparison, the results from Exp 587 and Exp 590 are not considered for the calibration of simulation tool in the following chapter.

	40 Hz	50 Hz	60 Hz
10 RPM	0.326 (Exp 587*)		
16 RPM	0.312 (Exp 566)	0.315 (Exp 561)	0.281 (Exp 560) 0.256 (Exp 563*) 0.295 (Exp 590*)
25 RPM			0.292 (Exp 564) 0.285 (Exp 592)

Table 7: Friction coefficient μ for all experiments
* denotes experiments that are disregarded in further analysis

In the Table 7 and Figure 23, it is shown that the friction coefficients from Exp 563 and Exp 587 deviates the most from other experimental data. Theses mean that sharpness of the tool and cutting performance is very different in Exp 563 and Exp 587, comparing to rest of the data. Because the aim of the modelling is to establish numerical model when tool state and controlled force are stable. Thus, results from Exp 563 and Exp 587 are not considered for the following numerical modelling and calibration of simulation tool.

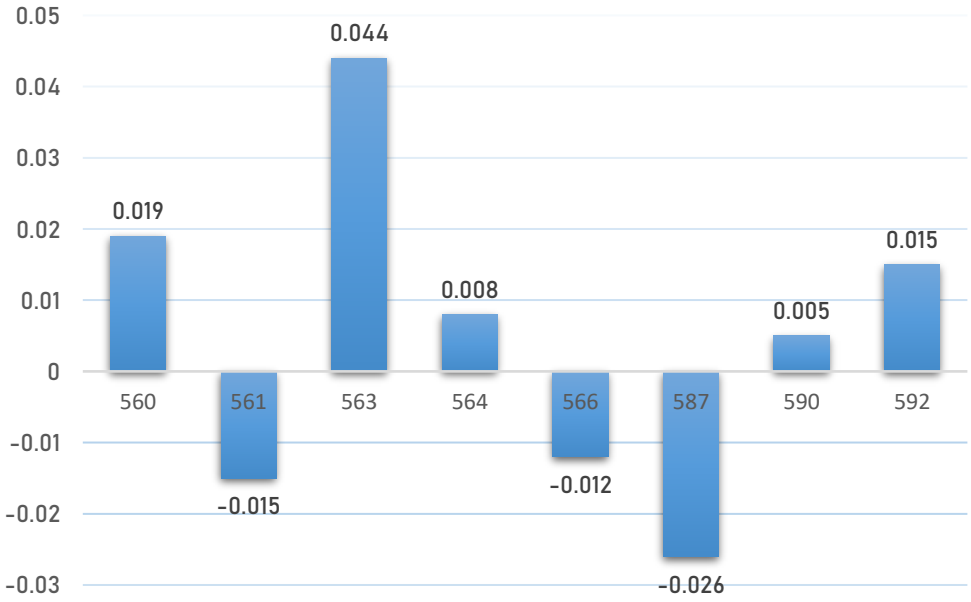

Figure 23 Deviation of friction coefficient from average friction coefficient: 0.3

3.4.2 Validation of the rail grinding process model in iBRUS

Before using simulation tool to predict energy consumption, it's important to validate that the simulation data is a close representation of experimental data. Toenshoff and Denkena [24] reported that, in a cutting process, the relationship between undeformed chip thickness and specific cutting force can be approximated by a straight line when plotted in a double logarithmic scale, as shown in

Figure 24. When looking at the simulation data, this relationship was also observed in the simulation results, as depicted in Figure 25.

Further examing the numerical model displayed in Figure 25, based on the calculated P-value, it can be concluded that the null hypothesis, which assumes that there is no statistically significant relationship between the predictor variable ($\log(a_p)$) and the response variable ($\log(K_c)$), is rejected. The low P-value of 0.005 indicates that the probability of the null hypothesis being true is less than 0.5%. Therefore, it is reasonable to assume that the same regression model will hold for a larger set of simulation data. Furthermore, the R-value of approximately -0.68 indicates that the model can explain almost 70% of the variability in the outcome data. The R-value in this context demonstrates a high degree of correlation, nearing a value of 0.7, a threshold commonly recognized as indicative of substantial model fit. In order to get more precise coefficients, more experiments would need to be performed.

Hence, it can be concluded that the forces exhibit similar behaviour in the simulation and in reality. The consistency between the experimental and simulation results suggests that the simulation model is capable of accurately capturing the physical phenomena of the cutting process.

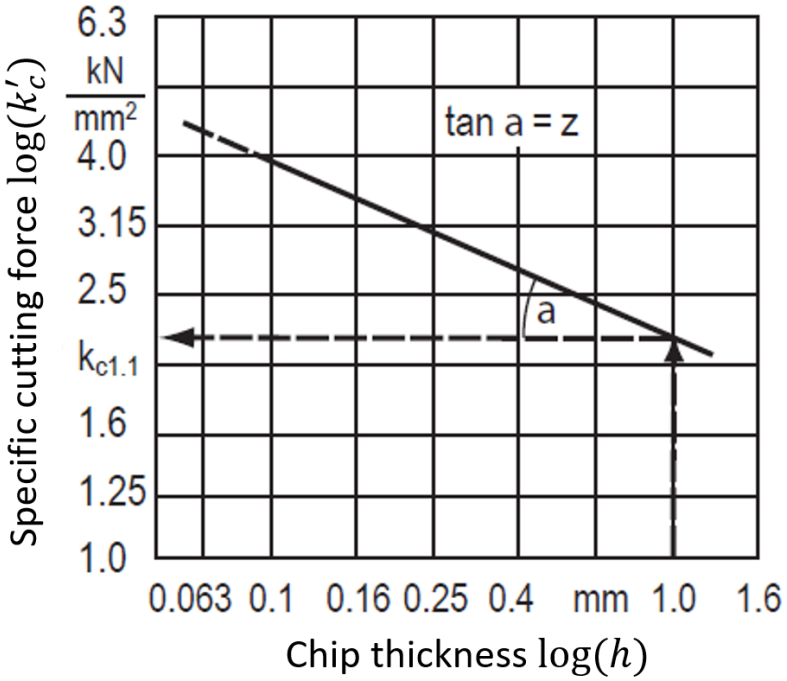

Figure 24: Chip thickness against specific cutting force,
where z is the exponential decrease in the specific cutting force

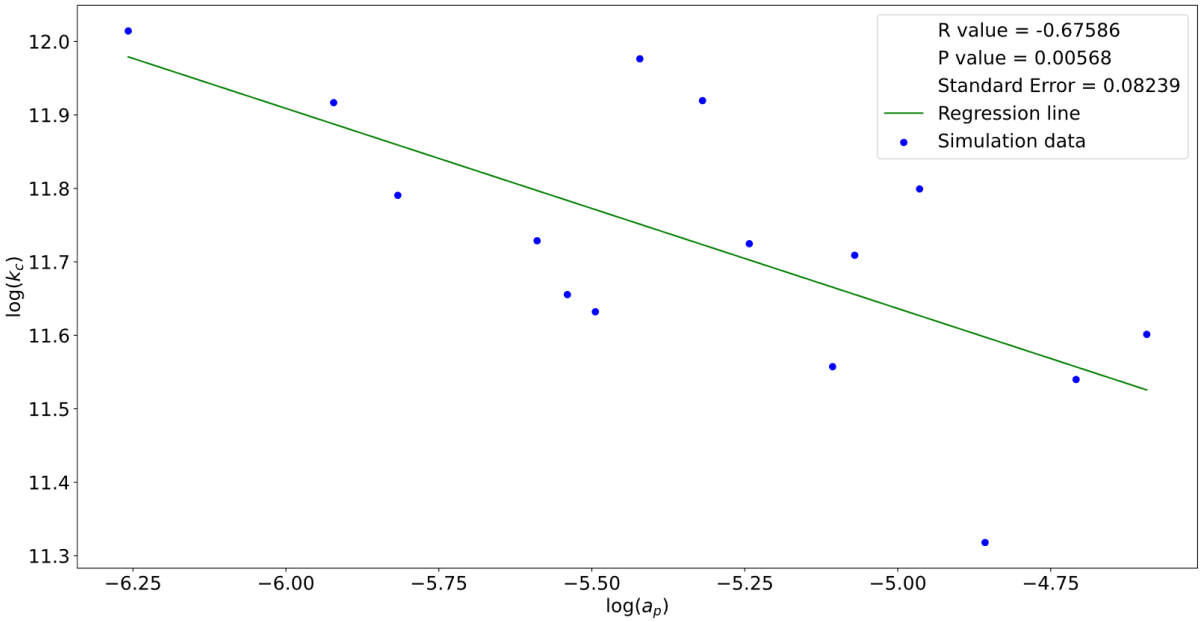

Figure 25: Double logarithmic plot of depth of cut against specific cutting force

3.4.3 Energy consumption prediction

The specific energy consumption, for experimental and simulation data is plotted in Figure 26. The cross represents simulated data, the cube represents experimental data.

The simulated energy consumption is lower than the experimental energy consumption. This is due to various reasons: such as the wear phenomena is not perfectly represented in the simulation, which will affect the friction coefficient of the tool, and thus affects the energy prediction. It is important to be noted that the specific energy calculated and plotted here only represents the energy spent for cutting. All the other components of energy consumption, shown in Equation (1) in section 1.3 is not quantified.

In Figure 26, three different set of data can be seen, represented by three colours. One colour stands for one cutting speed. The feed speed is increasing along the x-axes and the energy per removed volume is on the y-axes. It can be clearly seen that for every cutting speed, an optimal point exists somewhere between 1600 and 1800 mm/s of feed speed. This provides the direction of the search for optimal process parameters in the following chapter.

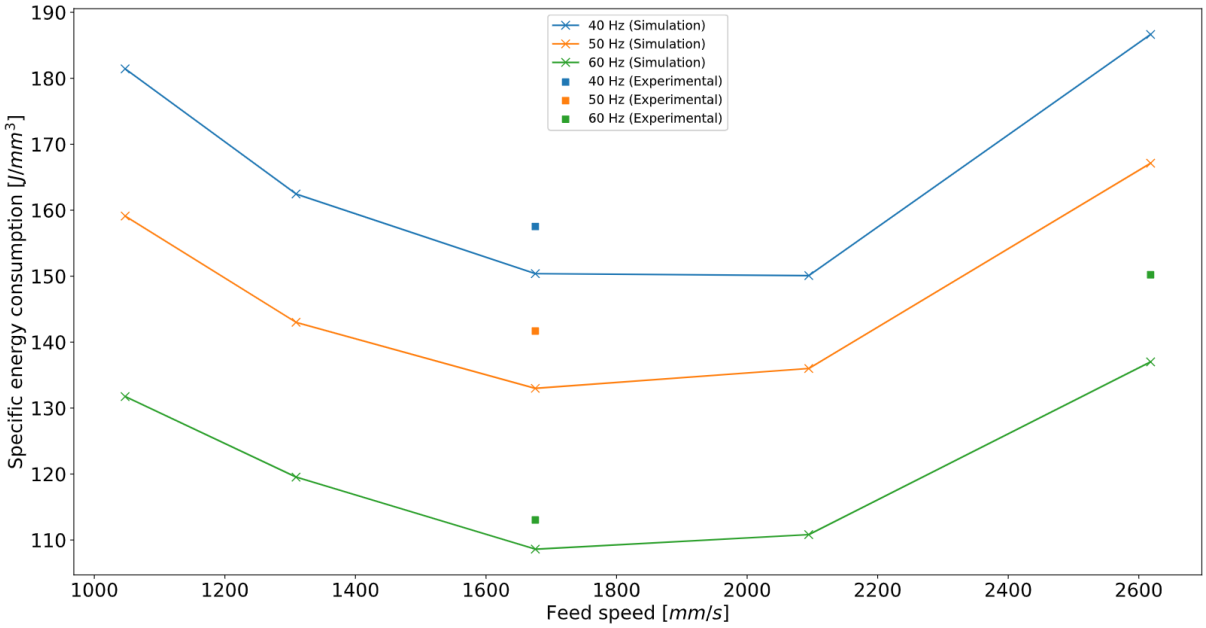

Figure 26: Feed speed against specific energy consumption for different spindle frequencies

It's also shown in Figure 27, that the grinding process gets more efficient with higher spindle frequency. For every feed speed simulated, the trend is the same. The specific energy consumption gets lower with higher spindle frequency.

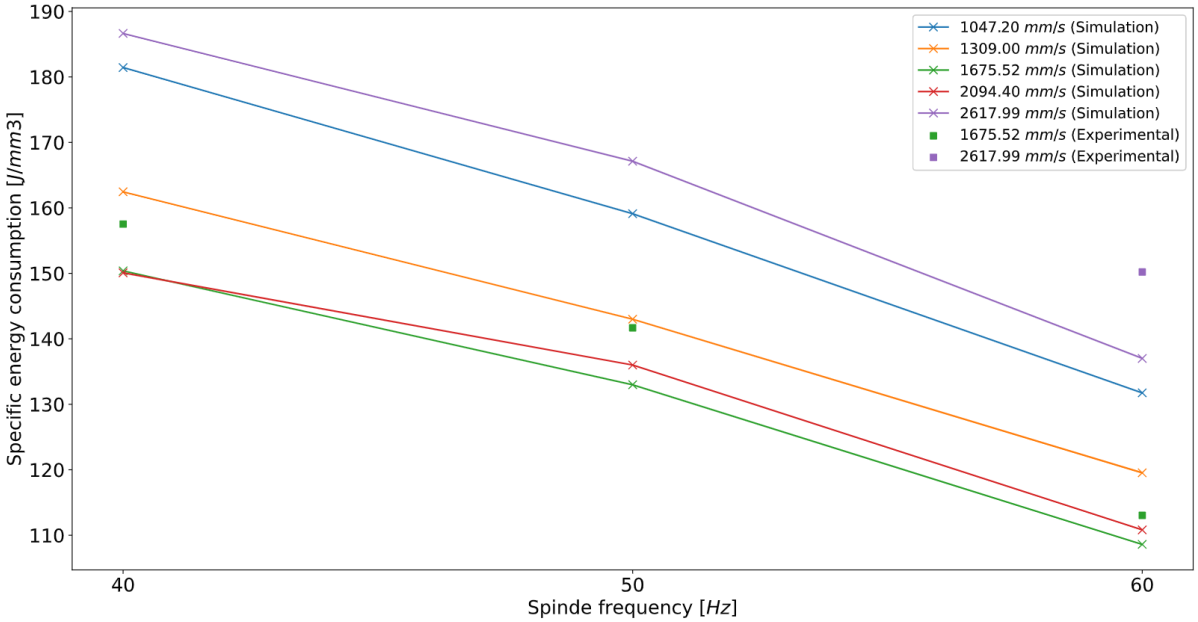

Figure 27: Spindle frequency against specific energy consumption for different feed speeds

3.5 Energy consumption optimization

In Section 3.5, the process of improving energy efficiency in rail grinding by adjusting certain parameters is discussed. The process is represented by a three-dimensional matrix with three main factors: feed speed, spindle frequency respectively cutting speed and normal force.

3.5.1 Optimization of feed speed

The initial phase of optimization in the rail grinding process was focused on the parameter feed speed. Feed speed, as a critical variable, exerts a direct impact on the depth of cut within the specified grinding operation. It is important to note that an increased feed speed results in a reduced depth of cut. According to Equation (11), a decrease in depth of cut will increase the specific energy consumption. In turn, increased feed speed will decrease specific energy consumption. This relationship suggests that an optimal feed speed value that would minimize specific energy consumption exists.

In order to ascertain this optimal feed speed value, a series of simulations were conducted, encompassing various feed speed conditions. The resulting data points were then used to construct a mathematical model, which facilitates the identification of the optimal feed speed value that corresponds to the lowest specific energy consumption.

The mathematical model constructed in this optimization process aids in the discovery of trends and patterns within the data, providing a robust and reliable method for the determination of the optimal feed speed.

As it can already be seen in Figure 26 in the last section 3.4.3, the optimal feed speed should be in the region from 1600 to 2000 mm/s. Therefore, more simulations have been performed for values in this range. Since the curves for different spindle frequencies look very similar, these simulations have been only performed for one spindle frequency, namely 60 Hz. The results of these simulations are presented in Figure 28.

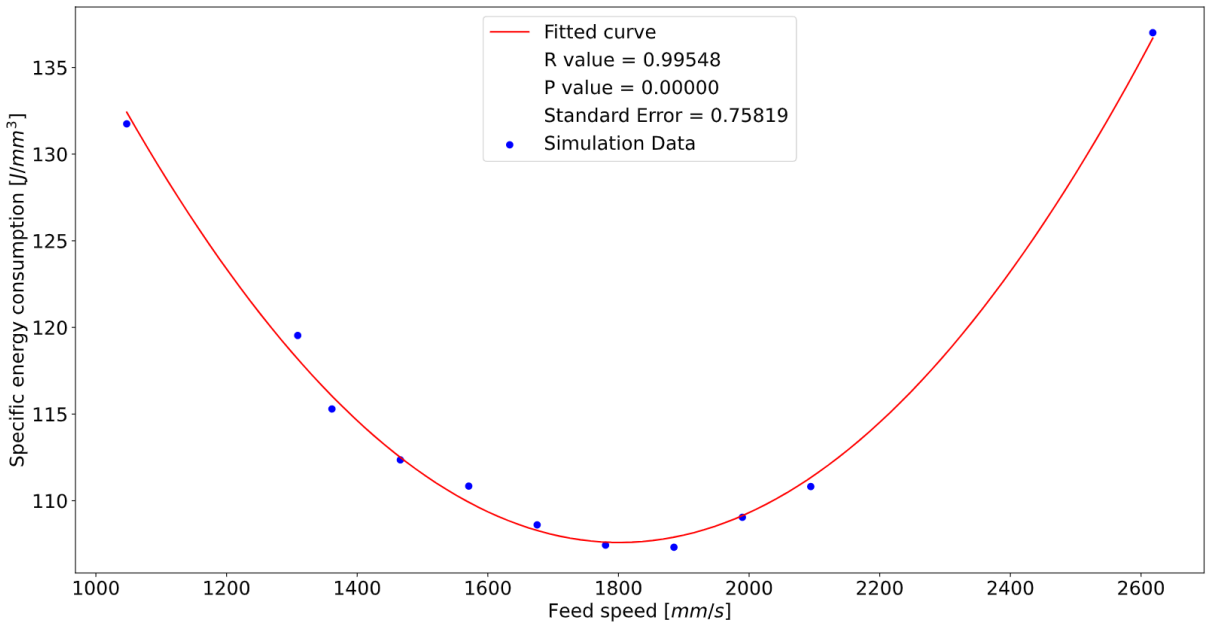

Figure 28: Simulation data for feed speed optimization for a spindle frequency of 60 Hz

Looking at the data, it is clear that a polynomial curve of degree two should be a good fit. The fitted curve is described by Equation (12).

$$y = 0.0000436 * x^2 - 0.157 * x + 249.2 \quad (12)$$

Where x is the feed speed and y is the specific energy consumption. Minimizing this equation with a respect to x results in an optimum feed speed of 1801 mm/s which yields a specific energy consumption of 107.6 J/mm^3 for a spindle frequency of 60 Hz.

3.5.2 Optimization of cutting speed (spindle frequency)

The second axis of optimization in the rail grinding process pertains to the cutting speed. Cutting speed exhibits an inverse relationship with the depth of cut compared to feed speed. A high cutting speed corresponds to an increased depth of cut. This phenomenon can be attributed to the fact that, for a constant feed speed, a higher cutting speed results in a greater number of grain-workpiece intersections per unit surface area. This, in turn, leads to an enhanced rate of material removal and ultimately, a deeper depth of cut.

As indicated by Equation (11), cutting speed appears in the numerator while the depth of cut a_p is situated in the denominator. To achieve a reduction in energy consumption, it is necessary for the numerator to decrease or the denominator to increase. Consequently, as long as the percentage change in the depth of cut is greater than the change in cutting speed, the specific energy consumption will exhibit a declining trend. This pattern is seen by the data presented in Figure 27 and further proven by the data in Figure 29.

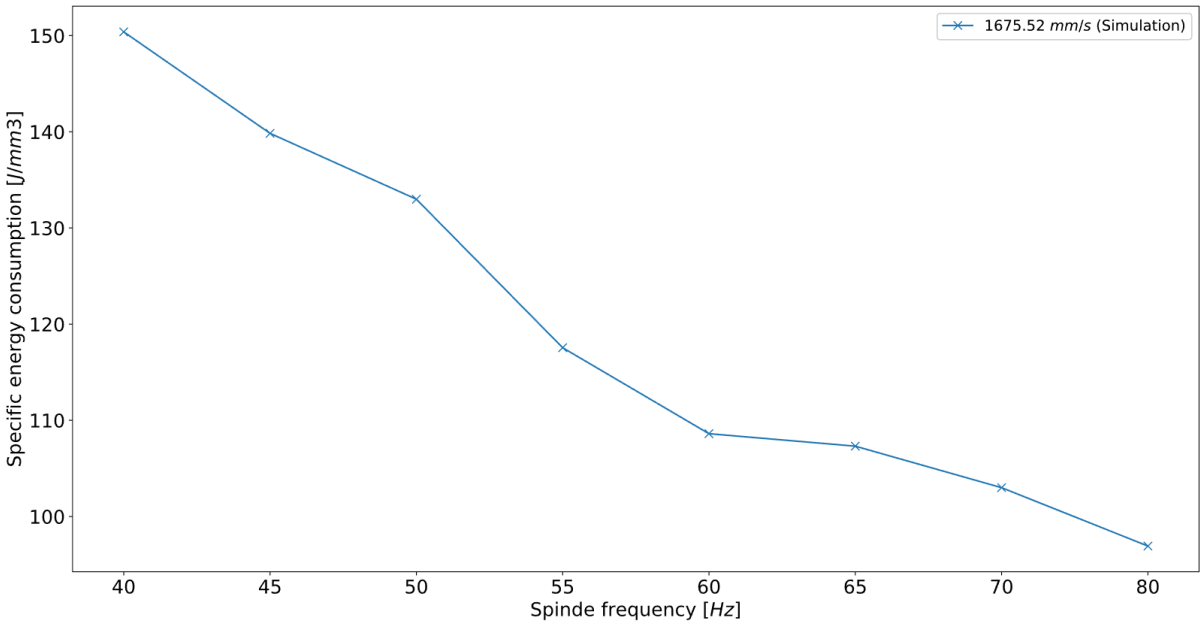

Figure 29: Spindle frequency against specific energy consumption.

3.5.3 Optimization of normal force

In order to optimize specific energy consumption with respect to normal force, it is crucial to establish a relationship between normal force and depth of cut within the context of rail grinding operations. A thorough review of existing literature reveals a lack of documented relationships between these two parameters, thereby necessitating the conduction of additional experiments to explain this connection.

Subsequently, a series of experiments were undertaken using the Olga test bench to investigate the dependency of normal force and depth of cut, as it's shown in Section3.4.1. Regrettably, the data obtained from these experiments proved inconclusive and insufficient for the establishment of a robust relationship between the two variables. The precise factors contributing to the unsuccessful nature of these experiments remain unclear. Further discussion of these experimental results is presented in the discussion section 4.5

3.5.4 Combined Optimization

Integrating the findings derived from the analyses presented in Sections 3.5.1 and 3.5.2 enables the formulation of a comprehensive optimization outcome for rail grinding operations. This consolidation of the identified parameters gives a better understanding of the relationships between feed speed, and spindle frequency, thereby facilitating the optimization of specific energy consumption.

To exemplify the efficacy of this unified optimization approach, a series of simulations were conducted using spindle frequencies of 70 Hz and 80 Hz, in conjunction with a range of feed speeds centred around 1800 mm/s. Since there exist preliminary experiments with spindle speed of up to 80 Hz, it can be said that these parameters are at the minimum feasible to test. These simulations were designed to explore the combined effects of the selected parameters on rail grinding performance, with the ultimate goal of identifying the optimal combination that yields the lowest specific energy consumption.

The outcomes of these simulations are visually represented in Figure 30, which illustrates the interplay between feed speed and spindle frequency. The numerical results are presented in Table 8.

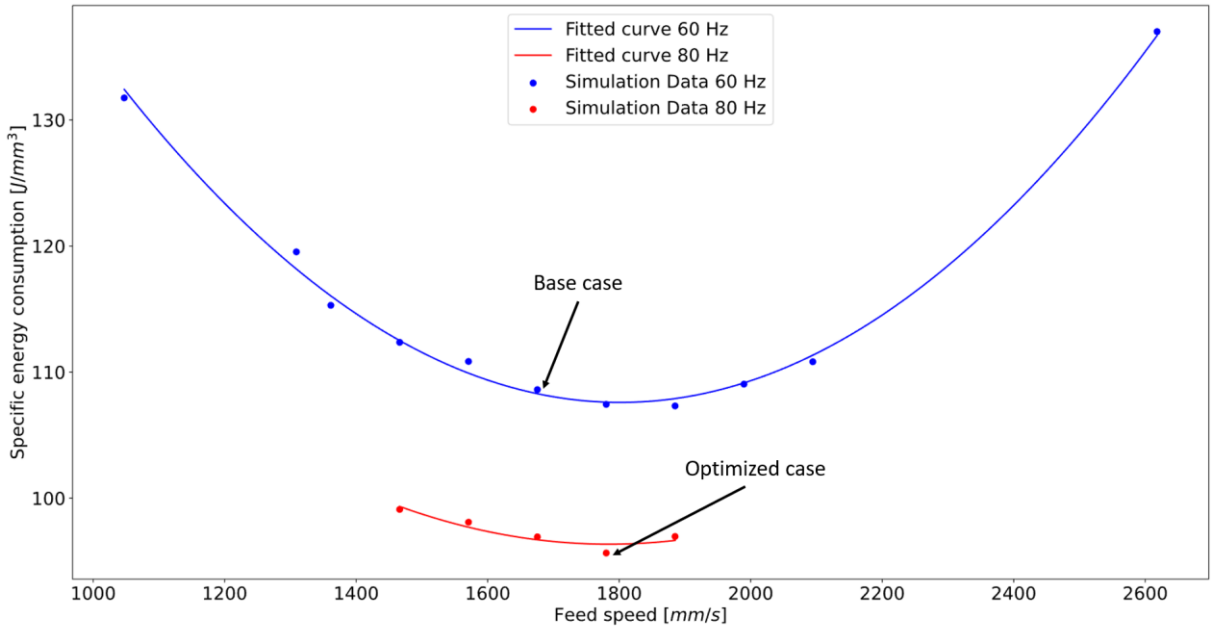

Figure 30: Results of specific energy consumption optimization

With both parameters optimized, a saving in specific energy consumption of about 12 % can be achieved.

	Feed speed	Spindle frequency	Specific energy consumption	Saving
Base case	1670 mm/s	60 Hz	108.61 J/mm3	-
Optimized case	1801 mm/s	80 Hz	95.64 J/mm3	11.9 %

Table 8: Results of specific energy consumption optimization

In the interest of thorough analysis, two additional simulations were conducted. These simulations were designed to evaluate the specific energy consumption associated with optimized spindle frequencies and feed speeds of 3300 mm/s and 4190 mm/s. It should be noted that the target feed speed of 4190 mm/s aligns with future objectives set forth by the grinding train manufacturer, Scheuchzer. The results derived from these simulations can be found in Table 9.

	Feed speed	Spindle frequency	Specific energy consumption	Loss
Base case	1670 mm/s	60 Hz	108.61 J/mm3	-
Moderate feed speed	3299 mm/s	80 Hz	127.08 J/mm3	17.0 %
Fast feed speed	4189 mm/s	80 Hz	151.84 J/mm3	39.8 %

Table 9: Specific energy consumption for faster feed speeds

The data analysis reveals that the specific energy consumption for elevated feed speeds surpasses that of the baseline condition, leading to a reduction in efficiency that may exceed 39%. In other words, it is not recommended to grind at elevated feed speed when using the common rail grinding wheel since that would lead to a higher specific energy consumption.

4 Conclusions

4.1 Single-grain scratch results

The removed volume results compared against the number of simulation steps showed that at least 30 simulation steps are needed per tool rotation to get satisfactory results. This is because when the rotational trajectory of grains is modelled with not enough simulation steps, the distance between two simulation steps deviates too much from the arc trajectory, which then leads to unsatisfactory material removal results.

The results from the single-grain scratch simulation showed a very robust removed volume against workpiece resolution. From the range of variation selected for workpiece resolution, it has shown a satisfactory material removal deviation that is around 5.16%, which is lower than the 10% target of this work package. The simulation step size chosen for this simulation was 60 steps per revolution. And it is shown that the workpiece resolution does not have a big effect on the single grain simulation. The deviation shows more like an offset behaviour, which needs to be further investigated.

In summary, achieving satisfactory material removal in simulations requires at least 30 steps per tool rotation, and while the workpiece resolution has minimal impact on single-grain scratch results, the observed deviation suggests that further investigation is needed.

4.2 Energy and temperature models results

The implemented energy and temperature model successfully delivers results. The temperature and energy results based on a single grain are not trivial to verify by comparing to the literature. In addition, those results are highly dependent on the process parameters, grinding wheel design and workpiece material.

The study of grinding burn by Lin et al. [19], Figure 19 showed the typical temperature profile during rail grinding as seen in Figure 31..

.

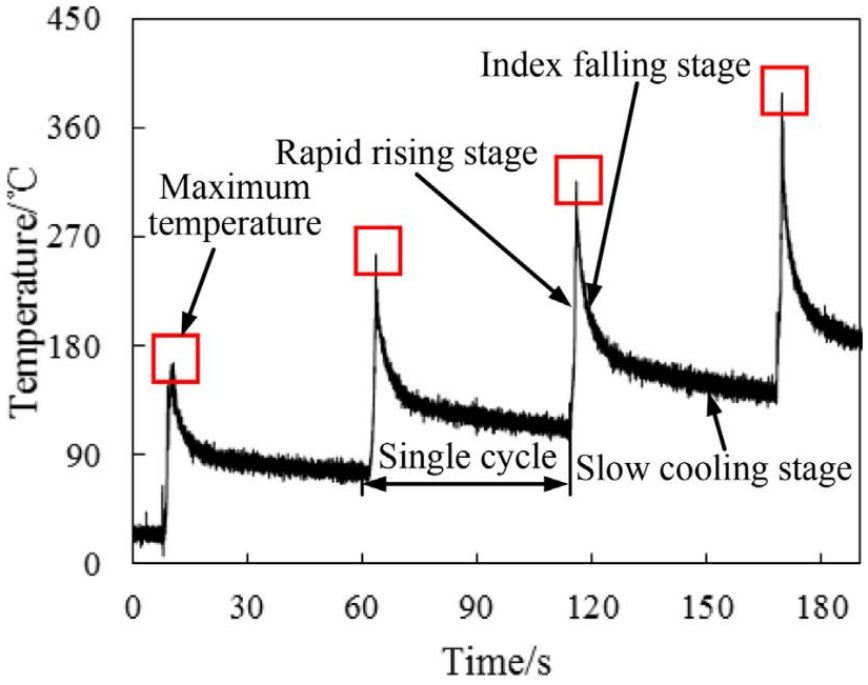

Figure 31 Typical grinding temperature curve [19]

Since the Takazawa temperature model gives the maximum temperature rise at the surface, before heat is dissipated, it doesn't give the workpiece temperature after heat dissipation. This makes it difficult to quantify the total amount of heat generated in the cutting process because the energy partition ratio available in the literature is only for the ratio between the heat dissipated into the workpiece and the total amount of heat generated.

The required energy result is not easy to verify with literature, since there aren't many published data focusing on energy consumption by a single grain. Comparing the cutting force of this single grain, shown in Fehler! Verweisquelle konnte nicht gefunden werden. to the experimental results available at inspire AG, the modelled cutting force is very close to reality.

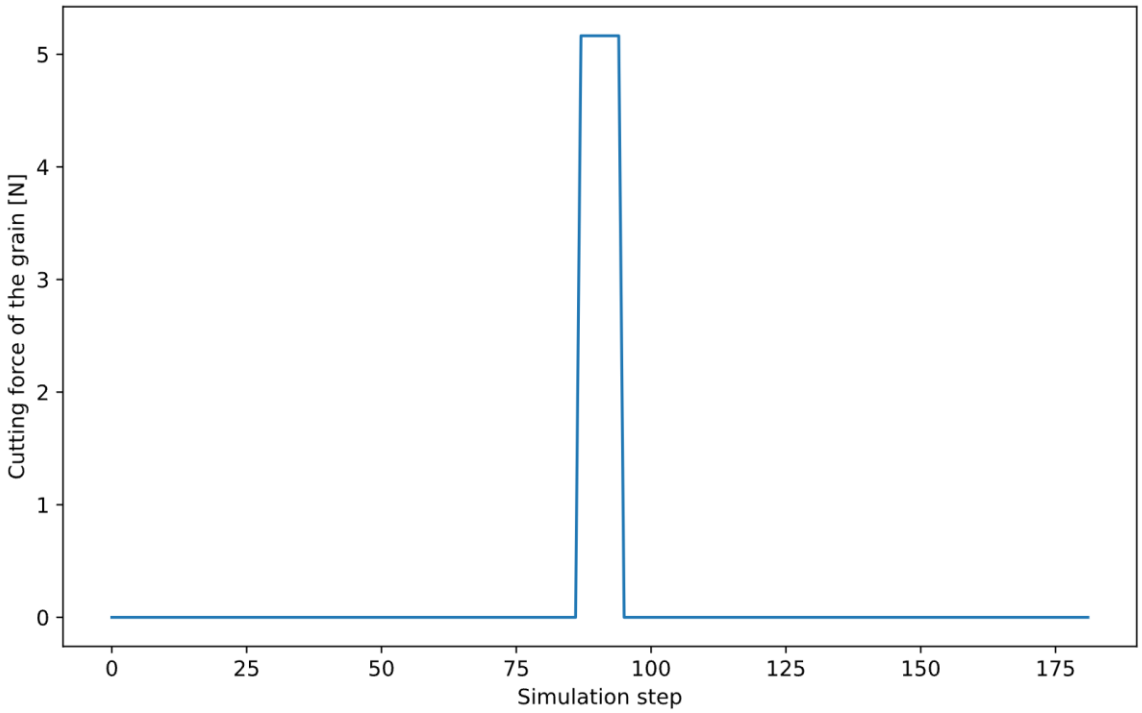

Figure 32 Grain cutting force

In various literature and most of the thermal models, it's assumed all grinding power becomes heat in the end [12][20]. While there are other findings, from Trigger and Chao [21], proposed that there is 3% of total grinding energy expanded by plastic deformation may not be converted to heat

To optimize the energy efficiency in grinding, this provides two potential ways to go forward: to decrease the portion of total cutting energy expanded that get transferred to heat, or to reduce the total cutting energy itself. The second strategy needs new wheel design that involves different grain orientation, grain distribution, and specific process parameters that gives the optimal wear progression rate which maintains the cutting efficiency in the process as long as possible.

In conclusion, while the energy and temperature model yields promising results, its validation against literature presents challenges due to variability in process parameters and limited data on single grain energy consumption. Future optimization avenues lie in energy efficiency enhancements, either by minimizing heat transfer from cutting energy or through innovative wheel designs that prolong cutting efficiency.

4.3 Energy prediction result

The difference between the simulated and experimental energy per volume result is due to the difference of simulated cutting force and experimental cutting force. In the experiment, since it's a force-controlled process, the cutting force is dependent on friction coefficient and normal force, as shown in equation (13).

$$F_{c\_exp} = \mu \cdot F_{N\_exp} \tag{13}$$

From all experiments, the mean of the friction coefficients, resulting to 0.291 was taken as input to simulation. While in reality, the friction coefficient has a deviation of 0.025 on average, as it's shown in

the table 4. Since the simulation has been calibrated in a way that the normal force of the simulations matches the normal force of the experiments, the cutting force of every simulation will have the same value if the same friction coefficient is applied. In reality however, the cutting force differs from experiment to experiment since the friction coefficient is never exactly the same.

$$F_{c,sim} = \sum_{i=1}^{n} k_c \, A_{cut,i} \tag{14}$$

	40 Hz	50 Hz	60 Hz
10 RPM	0.295 (Exp 587)		
16 RPM	0.312 (Exp 566)	0.315(Exp 561)	0.281 (Exp 560) 0.256 (Exp 563) 0.295 (Exp 590)
25 RPM			0.292 (Exp 564) 0.285 (Exp 592)

Table 10: Friction coefficients from experiments

In simulation, the tool cutting force is the sum of the cutting forces from all grains. For each grain, a simplified Kienzle force model is used as it's shown in equation (14). Ideally each grain has a corresponding k_c value. However, here the same k_c value is used, which underrepresents the deviation in k_c. Thus, the deviation of F_c is also underrepresented by $F_{c,sim}$.

In summary, the disparity between simulated and experimental energy per volume arises from the variability in friction coefficients in real-world experiments, and the use of a singular value for k_c in simulations which doesn't capture its inherent deviation, leading to an underrepresentation in simulated cutting force which in turn translates to a deviation in energy consumption.

4.4 Energy consumption optimization result for feed speed and cutting speed

The main goal of this research is to improve the energy efficiency of the rail grinding process, specifically by reducing spindle power consumption by at least 10%. Through adjustments to the feed and cutting speed, the study successfully achieved a significant reduction of nearly 12% in spindle power consumption. This section aims to explore the practical applicability of these findings under specific operating conditions and to address any remaining uncertainties that might affect the implementation of these optimizations.

.

As detailed in Sections 4.5, optimization of the normal force was not possible. Given that the normal force is anticipated to have a significant impact on the depth of cut, grinding efficiency, tool wear, and consequently on spindle power consumption, the results presented are only valid for a normal force of approximately 1330 N. This limitation stems from the depth of cut prediction model, which is based on a set of experiments with an average normal force of 1330 N. A deviation in normal force could lead

to substantial changes in the depth of cut, potentially altering the depth of cut prediction model significantly.

Another source of uncertainty lies in the validity range of the depth of cut model. It is likely that the depth of cut does not maintain a linear relationship with either feed speed or cutting speed. Because depth of cut cannot infinitely increase or decrease, along the change of cutting speed or feed speed. Nonetheless, due to insufficient experimental data, a linear model is employed, as it's shown in Figure 33. The point at which this linear model ceases to accurately represent reality remains uncertain.

Identifying this critical point presents a considerable challenge and often requires extensive experimentation. While a linear regression model is useful for grasping overall trends, it may not fully capture the intricate complexities and nonlinearities inherent in the rail grinding process. To accurately determine the cutting speed at which the specific energy consumption is minimized, a more sophisticated model or experimental design is necessary. This design should encompass a broader range of cutting speeds and their corresponding effects on the depth of cut. By doing so, we can better pinpoint the precise cutting speed that optimizes specific energy consumption during the rail grinding process.

After examining the experimental results in Section 3.4, it becomes apparent that the friction coefficient remains nearly constant for all experiments. This indicates that the grinding wheel maintained a consistent state throughout the investigated periods, implying a constant sharpness of the wheel's grains. Since the sharpness of the wheel significantly affects the depth of cut and grinding forces, the presented results are valid for the steady-state phase of the grinding process, during which the friction coefficient remains around 0.3.

Considering that the steady-state phase constitutes the majority of the grinding process duration, it can be inferred that other states of the grinding process have a minimal impact on spindle power consumption. Consequently, when the power-saving measures are applied to all states of the grinding process, there might be a slight reduction in power savings, albeit not substantial. Nevertheless, the overall impact on power consumption remains promising, especially during the steady-state phase, which represents the dominant part of the grinding process.

Besides enhancing energy efficiency, the pairing of the optimal process parameters (80 Hz and 1801 mm/s) carries the potential risk of inducing grinding burn. Due to the scarcity of research on predicting grinding burn based on process parameters, it becomes essential to conduct experimental validation. This is only possible outside the project as the novel grinding wheel for 80Hz needs to be designed, manufactured and tested first by the grinding wheel manufacturer. The primary objective of this validation is to assess whether the resulting workpiece surface meets the required standards or not. Consequently, this aspect must receive significant attention in the upcoming work package.

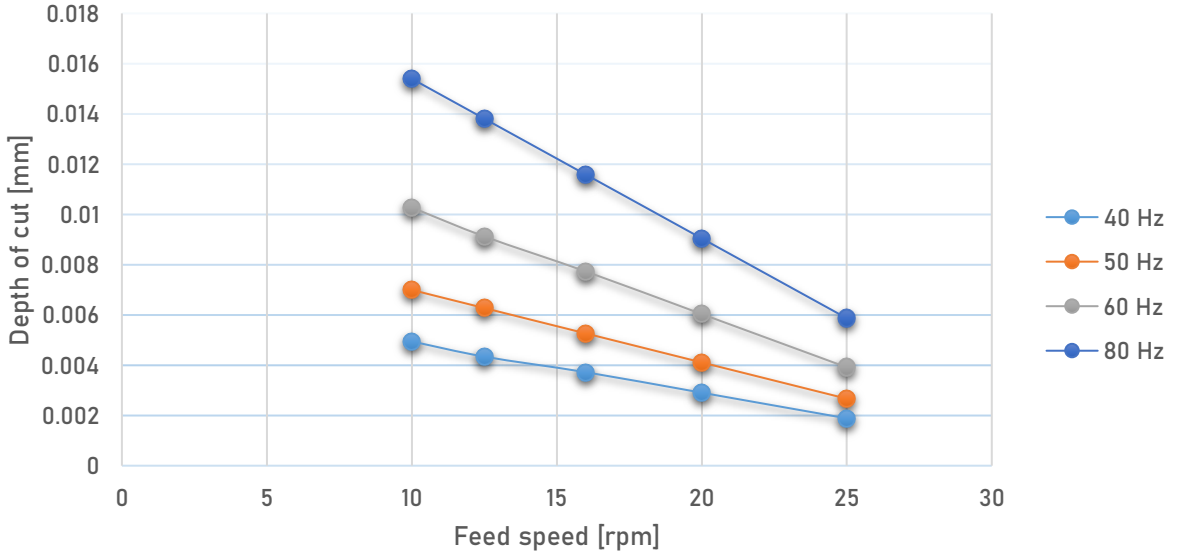

Figure 33: Dependency of feed and cutting speed on depth of cut

The data in Figure 33 suggests that the efficiency of the process decreases as the feed speed increases. To maintain the same level of efficiency at these high feed speed cases, certain adjustments would need to be made. For example, to achieve the same energy efficiency found when the feed speed is 1801 mm/s and the spindle frequency is 80 Hz, the spindle frequency would need to be significantly increased, reaching into the hundreds of Hz. However, such a high frequency is not currently feasible. Attempts to operate at these elevated spindle frequencies with the current tools would likely lead to equipment failure, as observed in early experiments. One possible solution to enhance energy efficiency at high feed speeds could be to modify the tool design.

In conclusion, while significant progress has been made towards enhancing the energy efficiency of the rail grinding process, several key considerations — including the constant normal force, non-linearities in the depth of cut model, and the potential for grinding burn — underline the necessity for further experimental validation and potential tool redesign to fully capitalize on the achieved power savings. However, due to constraints in time and resources, the focus has been redirected towards finding the optimal process parameters for the most commonly used tool rather than designing new grinding wheels.

4.5 Experimental results with different force

The second set of experimental results aiming to collect results at 1600 N didn't produce satisfactory results. The reasons leading to these results also showcases the challenges in the research of rail grinding process.

Uncertainty in the force control unit

The contact of the workpiece and the grinding unit is controlled by two cylindrical guides and a pneumatic cylinder. To adjust the controlled force, the spindle motor current and pneumatic pressure are used as parameters for pressure adjustment to control the force. For targeted normal force of 1400 N, the set pressure is 2.7 bar. To achieve the normal force of 1600N, a 2.4 bar pressure is set.

However, the measured force in these set of experiments, 590 and 592, are all lower than the expected 1600 N. The reasons for this are not clear and are being investigated now. One guess is that the friction

on the cylindrical guides was unconventionally high which made the guides stuck. This could result in lower force transferred from the grinding wheel on the workpiece ring.

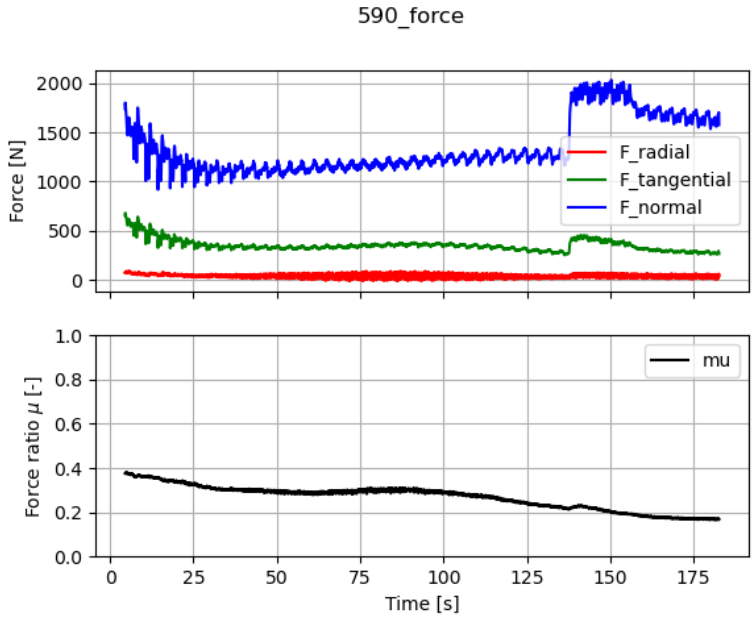

Figure 34 The force and friction coefficient measurement for experiment 590

Since the 59X set of experiments did not go as planned and produced unexpected results, they are not being used in calibration and optimization. This unfortunately prevented to establish a relationship between the normal force and depth of cut and therefore also optimization of the normal force.

Unexpected large depth of cut

One of the experiments conducted in the second set of the experiments is 587. The controlled force for 587 is expected at 1400 N. The aim of conducting the 587 experiment is to validate the relationship discovered between a_p and v_f. Under the condition that the state of the grinding tool is relatively the same, indicted by tool friction coefficient μ, the achieved depth of cut should not be far away from the one extracted from the linear regression done on the set of 56X experiments. However, as it's shown in the Table 11, the expected and the measured depth of cut are vastly different.

Experiment 587	Expected a_p based on correlation	Measured a_p
Depth of cut a_p [µm]	4.94	15.1

Table 11 Expected and measured depth of cut in experiment 587

One contributing factor to the observed phenomenon lies in the limitation of using the friction coefficient as the sole measure to represent the sharpness of the grinding tool. While the measured friction coefficients (μ) in all experiments were approximately 0.3, indicating a similarity in the overall sharpness of the tools, this metric fails to account for the intricate distribution of individual sharp grains on the grinding wheel surface. As a result, even though the overall sharpness appears similar, the arrangement and density of sharp grains may differ significantly between the grinding wheels used in the experiments.

For instance, if all the sharp grains are concentrated in a specific area on the grinding wheel, it could lead to localized high cutting forces and, consequently, a large depth of cut at that particular region. Conversely, if the sharp grains are more sparsely distributed across the wheel, the resulting depth of cut may not be as substantial.

In the context of the current set of experiments, the unexpectedly lower measured grinding force suggests that the grinding wheel utilized may possess higher sharpness compared to the wheel used in the initial set of experiments. This variation in sharpness could explain the differences in energy consumption and specific cutting forces observed between the two sets of experiments.

To gain a deeper understanding of the exact sharpness difference between two grinding wheels exhibiting the same friction coefficient, additional work is required. One approach could involve producing rail grinding tools in iBRUS with two different wheel profiles that have been meticulously matched for sharpness. By comparing these wheels and analyzing their respective effects on the resulting depth of cut and energy consumption, researchers can obtain valuable insights into how subtle variations in wheel profile impact the grinding process.

In conclusion, the friction coefficient, while informative to some extent, does not provide a complete picture of the sharpness of the grinding tool. The distribution of individual sharp grains on the wheel surface plays a vital role in the grinding process and can significantly influence the specific cutting forces, energy consumption, and material removal efficiency. Conducting further investigations and experiments is essential to enhance our understanding of this intricate relationship and optimize the rail grinding process for improved energy efficiency and performance.

5 Outlook and next steps

The primary objective of this study is to make substantial enhancements to the rail grinding process, with a specific focus on achieving a considerable reduction in spindle power consumption. The aim is to achieve a minimum reduction of 10%, which represents a significant improvement in the energy efficiency of the grinding operations.

To accomplish this objective, the study strategically adjusted the feed and cutting speed, seeking to identify the optimal combination that would lead to the most substantial power savings. Through rigorous experimentation and data analysis, the team successfully achieved a reduction of nearly 12% in spindle power consumption. This achievement marks a substantial step forward in optimizing the grinding process and aligning it with the broader goal of energy conservation and sustainability.

However, while the results are promising, the practical applicability of these findings under specific real-world conditions remain challenging due to the required higher cutting speed of 80 Hz. Additionally, the applicability of the identified optimizations may vary depending on various factors, such as the type of rail network, traffic volume, track conditions, and grinding equipment used. It is essential to evaluate how these optimizations translate into different operational scenarios and ensure that they can be effectively and safely implemented across diverse rail networks.

Factors such as potential variations in rail material properties, environmental conditions, and operational constraints could influence the feasibility and long-term viability of the proposed optimizations. Addressing and understanding these uncertainties is crucial for ensuring the practicality and reliability of implementing the identified power-saving measures.

In the rail grinding process, numerous interrelated factors influence the energy consumption, and accurately pinpointing the critical point where it is minimized requires a more nuanced approach. The linear regression model, while useful for providing a general understanding of trends, cannot fully account for the intricate and nonlinear relationships between the process variables.

The wheel's sharpness, for instance, directly impacts its cutting efficiency and the energy required to remove material from the rail surface. Additionally, the size of the contact area between the wheel and the rail, as well as the grinding forces involved, play crucial roles in determining the energy expenditure during grinding.

Moreover, the properties of the rail material itself, such as hardness and wear resistance, further contribute to the overall energy demand. These factors interact in complex ways, making it challenging to accurately model their combined effect on specific energy consumption using a linear approach.

To overcome these limitations and achieve a more accurate determination of the critical point, a more sophisticated model is necessary. Advanced modeling techniques, such as nonlinear regression, machine learning algorithms, or physics-based simulations, can better capture the complexities of the rail grinding process. By incorporating a wider range of cutting speeds and their corresponding effects on the depth of cut, the model can provide valuable insights into the precise cutting speed that optimizes energy consumption.

Furthermore, conducting extensive experimentation is vital for validating the model and fine-tuning its parameters. Designing a comprehensive experimental plan that covers a diverse range of operating conditions will help in developing a robust and reliable model.

In conclusion, while linear regression offers a useful starting point for understanding trends in the rail grinding process, its limitations necessitate the use of more sophisticated and comprehensive modeling techniques. Only by doing so can we accurately identify the critical cutting speed that minimizes specific energy consumption, thereby paving the way for more efficient and sustainable rail grinding practices.

Due to unforeseen challenges and experiences encountered during project execution some deviations from the original project plan needs to be addressed:

Normal Force Optimization: As mentioned in Section 4.5 optimizing the normal force proved to be challenging due to imperfect experimental data. The uncertainty and complexity of the grinding process led to difficulties in data collection. Therefore, normal force optimization might require more time and resources than initially anticipated. It is crucial for the project stakeholders to discuss and agree upon the need for continued work in this area.

Tool Optimization: The desired tool optimization to comply with Scheuchzer's preferred feed speed values could be more demanding than expected. Exploring different directions, such as grain size, shape, density, and grain orientation in the grinding wheel, necessitates extensive simulations and potential collaboration with grinding wheel manufacturers. As manufacturing these new, by simulation predicted grinding wheel, was not initially part of the project plan, the feasibility and long-term implications of such tool optimization need careful consideration. Unforeseen challenges during experimental validation and optimization could lead to significant time delays.

Collaboration with Partners and Manufacturers: The future project's success relies on close collaboration between inspire as research instituition, the grinding wheel manufacturer and grinding train operator. . Additional coordination and negotiations may be required to ensure that the implemented optimizations are practically feasible.

While deviations from the original project plan are addressed, they also present opportunities for improvement, adaptation a future common collaboration.

6 National and international cooperation

Collaborations with Scheuchzer SA is expected to continue after this project for the originally planned work packages 5 and 6. The findings of optimization work in the lab experiment and simulation will be communicated with Scheuchzer SA, in order to realize the plausibility of the solution early on.

In the scope of and the initially foreseen work packages 1-6, there is no cooperation with other entities yet.

7 Communication

There are no communications regarding this project.

8 Publications

There is no publication derived from the current project yet.

9 References

[1] Rowe, W. B. (2013). Principles of modern grinding technology, Chapter 16 William Andrew.
[2] Malkin, & Guo, C. (2008). Grinding technology : theory and application of machining with abrasives, second edition (2nd ed.). Industrial Press.
[3] Yoon, H.-S., Lee, J.-Y., Kim, H.-S., Kim, M.-S., Kim, E.-S., Shin, Y.-J., Chu, W.-S., & Ahn, S.-H. (2014). A comparison of energy consumption in bulk forming, subtractive, and additive processes: Review and case study. International Journal of Precision Engineering and Manufacturing-Green Technology, 1(3), 261–279. https://doi.org/10.1007/s40684-014-0033-0
[4] Hacksteiner, M., Peherstorfer, H., & Bleicher, F. (2018). Energy efficiency of state-of-the-art grinding processes. Procedia Manufacturing, 21, 717–724. https://doi.org/10.1016/j.promfg.2018.02.176
[5] OEC. (n.d.). Gear cutting, grinding and finishing machines. OEC. Retrieved May 6, 2022, from https://oec.world/en/profile/hs/gear-cutting-grinding-and-finishing-machines
[6] Swiss Federal Office of Energy SFOE. (n.d.). What is the energy strategy 2050? Startseite. Retrieved April 21, 2022, from https://www.bfe.admin.ch/bfe/en/home/policy/energy-strategy-2050/what-is-the-energy-strategy-2050.html
[7] Linke, B. S., Garretson, I., Torner, F., & Seewig, J. (2017). Grinding energy modelling based on friction, plowing, and shearing. Journal of Manufacturing Science and Engineering, 139(12).
[8] Energiekennzahlen. Swissmem. (n.d.). Retrieved February 28, 2022, from https://panorama.swissmem.ch/de/jahreszahlen-2019/energiekennzahlen.html
[9] SIGMATOOLS, inspire AG, SFOE. (n.d.). EE4MT. ee4mt. Retrieved December 21, 2021, from http://www.ee4mt.ch/
[10] Grizzly Picture: Retried Dec, 15, 2022, from https://tinyurl.com/mz5yzhxy

[11] Aggarwal, S., Nešić, N., & Xirouchakis, P. (2013). Cutting torque and tangential cutting force coefficient identification from spindle motor current. The International Journal of Advanced Manufacturing Technology, 65(1), 81–95. https://doi.org/10.1007/s00170-012-4152-x
[12] Shaw, M. C. (1996). Energy Conversion in Cutting and Grinding*. CIRP Annals, 45(1), 101–104. https://doi.org/10.1016/S0007-8506(07)63025-X
[13] Malkin, S. (1984). Grinding of metals: Theory and application. Journal of Applied Metalworking, 3(2), 95–109. https://doi.org/10.1007/BF02833688
[14] TAKAZAWA, K. (1966). Effects of Grinding Variable on Surface Structure of Hardened Steel. Bull. of Japan Soc. of Precision Engineering, 2(1).
[15] Kato, T., & Fujii, H. (1998). Temperature Measurement of Workpieces in Conventional Surface Grinding. Journal of Manufacturing Science and Engineering, 122(2), 297–303. https://doi.org/10.1115/1.538918
[16] Rowe, W. B., Black, S. C. E., Mills, B., Morgan, M. N., & Qi, H. S. (1997). Grinding temperatures and energy partitioning. Proceedings of the Royal Society of London. Series A: Mathematical, Physical and Engineering Sciences, 453(1960), 1083–1104. https://doi.org/10.1098/rspa.1997.0061
[17] Kuffa, M. (2017). High Performance Dry Grinding—HPDG (p. 175 p.) [ETH Zurich; Application/pdf]. https://doi.org/10.3929/ETHZ-B-000268402
[18] Weerasekara, N. S., Liu, L. X., & Powell, M. S. (2016). Estimating energy in grinding using DEM modelling. Minerals Engineering, 85, 23–33. https://doi.org/10.1016/j.mineng.2015.10.013
[19] Lin, B., Zhou, K., Guo, J., Liu, Q. Y., & Wang, W. J. (2018). Influence of grinding parameters on surface temperature and burn behaviors of grinding rail. Tribology International, 122, 151–162. https://doi.org/10.1016/j.triboint.2018.02.017
[20] Brian Rowe, W. (2017). Temperatures in Grinding—A Review. Journal of Manufacturing Science and Engineering, 139(12). https://doi.org/10.1115/1.4036638
[21] Trigger, K. J., & Chao, B. T. (2022). An Analytical Evaluation of Metal-Cutting Temperatures. Transactions of the American Society of Mechanical Engineers, 73(1), 57–66. https://doi.org/10.1115/1.4016141
[22] Singh, V., Venkateswara Rao, P., & Ghosh, S. (2012). Development of specific grinding energy model. International Journal of Machine Tools and Manufacture, 60, 1–13. https://doi.org/10.1016/j.ijmachtools.2011.11.003
[23] Gharaei, A., Wahl, T., Kuffa, M., and Wegener, K., 2022, Vorhersage der Werkstück-Oberflächenrauheit beim Hochleistungs- Trockenschleifen mittels Simulation, Zürich, Switzerland.
[24] Toenshoff, H. K., & Denkena, B. (2013). Basics of cutting and abrasive processes. https://doi.org/10.1007/978-3-642-33257-9

10 Appendix

In the appendix additional information is depicted that can help to understand certain technicalities better. These informations are not necessary to grasp the key findings but may be interesting to readers who want to dive deeper into the topic.

10.1 Work package 1

10.1.1 Experimental Setup

Figure 35 shows the 3D model of Olga test bench.

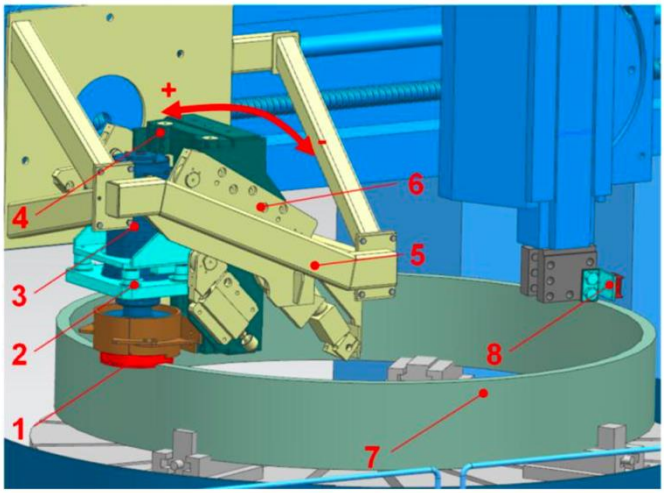

Nr.	Part
1.	grinding wheel
2.	force measurement system
3.	spindle motor
4.	vertical pneumatic cylinder
5.	frame
6.	milled slide
7.	workpiece
8.	laser sensor

Figure 35: 3D model of rail grinding test bench

Figure 36 shows how the workpiece is represented with various number of planes.

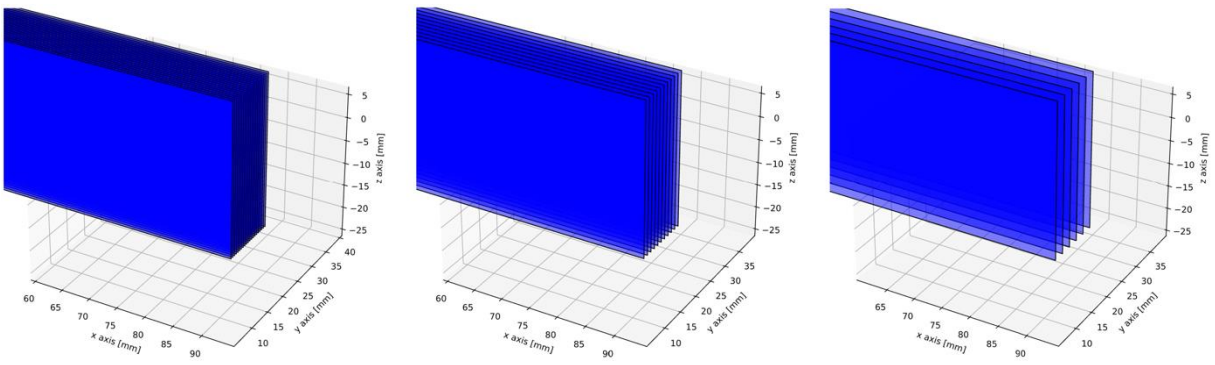

Figure 36 Illustration of different number of planes used for workpiece representation in iBRUS

10.2Work package 2

10.2.1 Two step data processing for experimental data

When raw data are collected, the time series shows the full profile from the tool is not yet cutting the workpiece, to the cutting process and until the end of the cutting process. First step of the data processing is cropping out the idle time, when tool is not grinding. After this step, the force result will look like Figure 37.

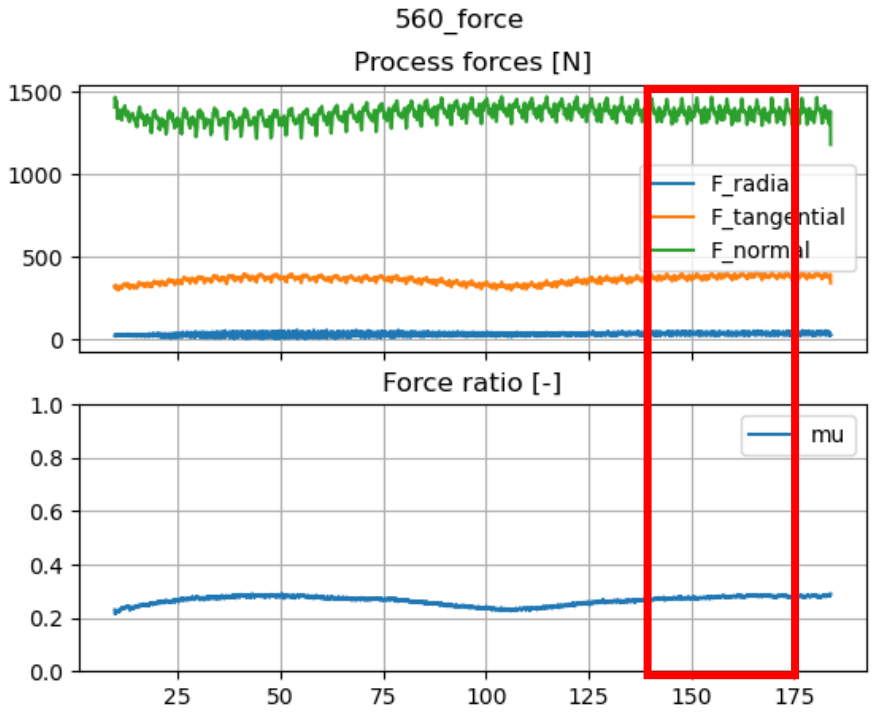

Figure 37 Force profile and friction coefficient of experiment 560

The second step of the data processing is to select a region of the time series, where friction coefficient is rather steady. A common friction coefficient found across various experiments is 0.3. Thus, a window of time series is selected where the friction coefficient doesn't oscillate much around 0.3. In the case of 560, the last 30s of the Figure 37 is selected and average of normal force F_N, friction coefficient μ is then calculated.

The same window is applied then on pre-processed cutting depth result from each experiment. And average value is then extracted based on the selected values in this window, as it's shown in the Figure 38.

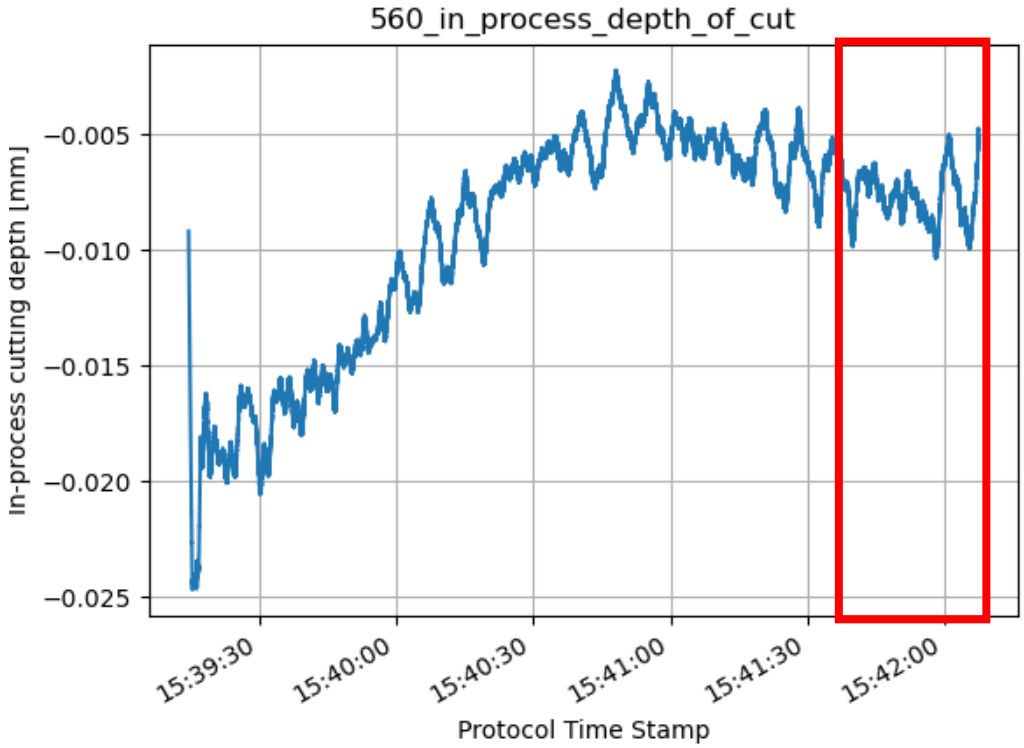

Figure 38 In process depth of cut in experiment 560

10.2.2 Experimental results

	40 Hz	50 Hz	60 Hz
10 RPM	15.14 µm (Exp 587)		
16 RPM	3.72 µm (Exp 566)	5.26 µm (Exp 561)	7.73 µm (Exp 560) 5.14 µm (Exp 563) 19.87 µm (Exp 590)
25 RPM			3.92 µm (Exp 564) 2.88 µm (Exp 592)

Table 12: Depth of cut a_p for all experiments

	40 Hz	50 Hz	60 Hz
10 RPM	1448.94 N (Exp 587)		
16 RPM	1246.51 N (Exp 566)	1254.76 N (Exp 561)	1374.29 N (Exp 560) 1385.60 N (Exp 563) 1158.98 N (Exp 590)
25 RPM			1395.93 N (Exp 564) 1229.97 N (Exp 592)

Table 13: Normal force F_N for all experiments

10.2.3 Discovery of dependencies between process variable: depth of cut vs specific cutting force kc

While processing simulation and experimental data, another set of dependencies are depicted in Figure 39 and Figure 40. These relationships could also provide insight on further optimization work. These two figures show, k_c and specific energy consumption exhibits similar dependencies with depth of cut. However, this result couldn't be used directly in the optimization work because k_c is dependent on material property of the workpiece and the grain, and as well the kinematics. Since iBRUS cannot simulate material property, the optimization of k_c couldn't be conducted.

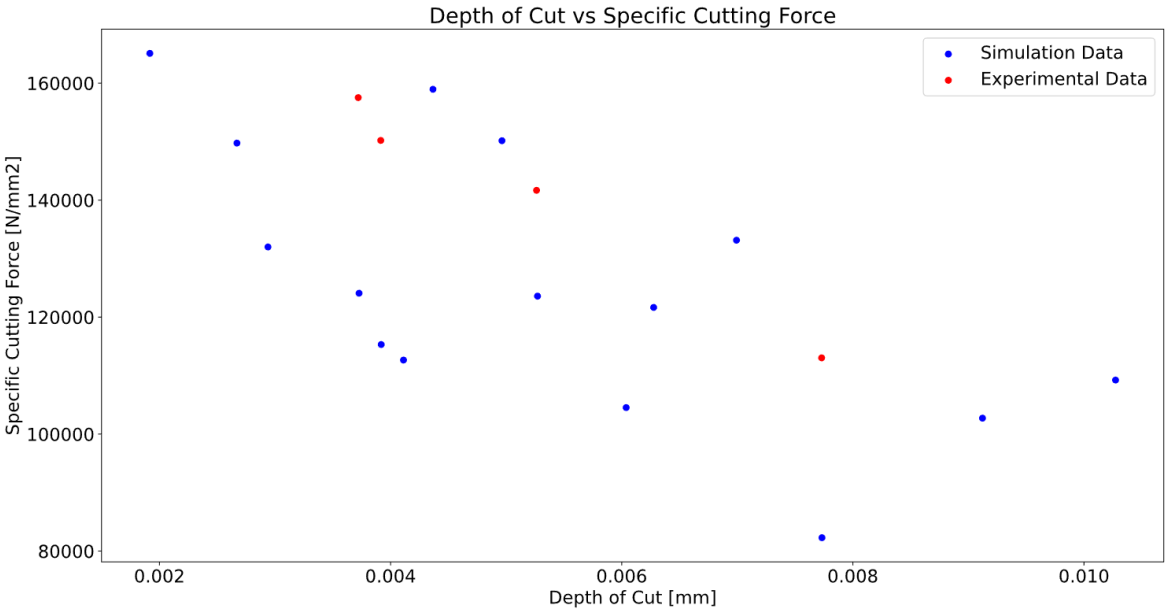

Figure 39 Dependencies between specific cutting force and depth of cut

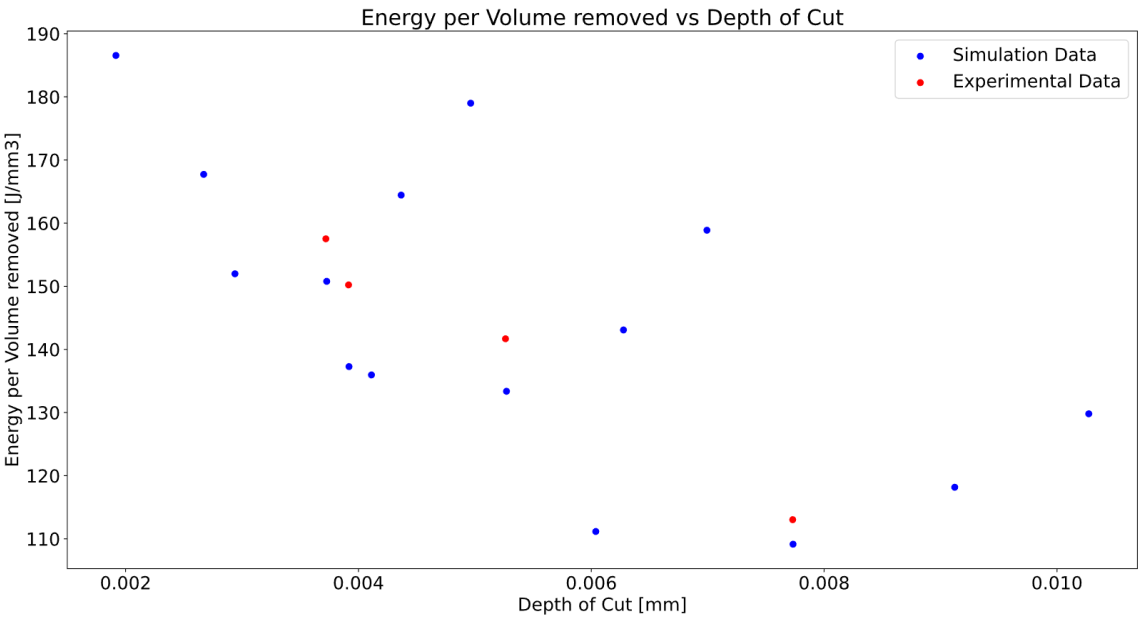

Figure 40 Dependencies between specific energy and depth of cut

10.3 Work package 3

10.3.1 Depth of cut prediction

By having a look at the depths of cut of Experiment 560 and 564 it can be seen that an increase of 9 rpm in feed speed, causes a decrease of 50.7 % in depth of cut. With that relationship the depths of cut for 40 Hz/ 25 rpm and 50 Hz/ 25 rpm can be calculated. They are indicated as red in Table 14. With two depths of cut for each spindle frequency on different feed speeds, a linear regression for each spindle frequency could be made in order to calculate all other depths of cut. The results from the linear regression are shown in Equations (15), (16) and (17).

$$a_{p,40Hz}\,[\mu m] = -0.204 \cdot v_f[rpm] + 6.98 \tag{15}$$

$$a_{p,50Hz}\,[\mu m] = -0.2886 \cdot v_f[rpm] + 9.88 \tag{16}$$

$$a_{p,60Hz}\,[\mu m] = -0.4339 \cdot v_f[rpm] + 14.51 \tag{17}$$

These equations allow for the calculation of every other possible combination of feed speed and spindle frequency in the feasible region, indicated as green numbers in Table 14.

In order to get depths of cut for spindle frequencies not displayed in Table 14, a linear regression has been done in direction of spindle frequency shift. An example of this is shown in Equation (18) which describes the relationship between the depth of cut and spindle frequency for a feed speed of 16 rpm.

$$a_{p,16rpm}\,[\mu m] = 0.2004 \cdot f_s[Hz] + 4.455 \tag{18}$$

		Spindle frequency		
		40 Hz	50 Hz	60 Hz
Feed speed	10 RPM	4.94 µm	6.99 µm	10.27 µm
	12.5 RPM	4.34 µm	6.27 µm	9.12 µm
	16 RPM	3.72 µm	5.26 µm	7.73 µm
	20 RPM	2.904 µm	4.11 µm	6.03 µm
	25 RPM	1.88 µm	2.67 µm	3.92 µm

Table 14: Depth of cut predictions